A Novel 3D Beam Domain Channel Model for Massive MIMO Communication Systems

Ji Bian, *Member, IEEE*, Cheng-Xiang Wang, *Fellow, IEEE*, Rui Feng, *Member, IEEE*, Yu Liu, *Member, IEEE*, Wenqi Zhou, Fan Lai, *Student Member, IEEE*, and Xiqi Gao, *Fellow, IEEE*

***Abstract*— Massive multiple-input multiple-output (MIMO) channels are distinctly characterized by their array non-stationarity, which has not been considered in the existing beam domain channel models (BDCMs). In this paper, the array non-stationarity of massive MIMO channels is modeled by the spatially consistent visibility regions (VRs) over a large uniform planar array (UPA) in terms of individual multipath components (MPCs). Based on this, a novel three-dimensional (3D) BDCM incorporating the effects of array non-stationarity is proposed. Statistical properties of the proposed BDCM including channel power, power leakage, space-time-frequency correlation function (STF-CF), and beam spread are derived. The ergodic and outage capacities are evaluated. The impacts of array non-stationarity on those statistics and channel capacity are analyzed. Results suggest that the beamwidths or spatial resolutions of the BDCM for different directions are not equal due to the array non-stationarity. This in turn increases the power leakage and correlation between channel elements and reduces the beam domain channel capacity.**

***Index Terms*— Massive MIMO systems, array non-stationarity, BDCM, GBSM, statistical properties.**

I. Introduction

MASSIVE multiple-input multiple-output (MIMO), or very large MIMO, plays an essential role in the fifth generation (5G) systems and will receive increasing attention in the future sixth generation (6G) systems due to its numerous merits, e.g., improving spectral efficiency, power efficiency, and physical layer security [1]. Meanwhile, the high frequency bands, i.e., millimeter-wave (mmWave) and Terahertz (THz) bands, have gathered great interests from researchers due to abundant available spectrum resources [2]. The severe path loss at high frequency bands can be overcome with the help of beamforming technique that generates narrow beams in specific directions. Besides, as the antenna number increases, the beamwidth becomes narrow, which decreases the inter-user interference and reduces the opportunity of eavesdropping [3]. The integration of massive MIMO and mmWave/THz communication technologies has become a consensus for future wireless communication systems [4].

In massive MIMO systems, the base station (BS) is equipped with large numbers of antennas, resulting in prohibitively high overhead of channel estimation and tremendous transceiver complexity. In [5], the beam division multiple access (BDMA) transmission scheme was proposed by transforming the massive MIMO channel from space domain into beam domain. As the number of antennas increases, channel elements tend to be uncorrelated and multipath fading disappears. The BS is able to simultaneously communicate with a certain number of user terminals (UTs) through non-overlapping beams. Thus, a multiuser channel can be decomposed into several single-user channels, which greatly reduces the transceiver complexity and channel estimation overhead [6]. Furthermore, as an emerging technology, reconfigurable intelligent surface (RIS) has the ability to change electromagnetic field in a customizable manner [7], [8]. However, the channel estimation is challenging since RIS is passive and the number of RIS elements is large. Note that the RIS channel exhibits a sparsity nature in beam domain. Therefore, the channel estimation can be treated as a sparse signal recovery problem and addressed by compressive sensing methods [9]. As the foundation of system performance evaluation, understanding the beam domain channel properties and developing realistic beam domain channel models (BDCMs) are indispensable.

A. Related Works

Due to large aperture size of the antenna array, massive MIMO channels are basically non-stationary in the array domain [10]. In [11], measurements were conducted at 5.8 GHz using a linear array and a square array. Results show that the channel experiences significant variations over

Manuscript received 12 August 2021; revised 2 February 2022 and 10 June 2022; accepted 31 August 2022. Date of publication 27 September 2022; date of current version 10 March 2023. This work was supported in part by the the National Key Research and Development Program of China under Grant 2018YFB1801101; in part by the National Natural Science Foundation of China (NSFC) under Grant 62101311, Grant 61960206006, and Grant 62001269; in part by the Key Technologies Research and Development Program of Jiangsu (Prospective and Key Technologies for Industry) under Grant BE2022067 and Grant BE2022067-1; in part by the Frontiers Science Center for Mobile Information Communication and Security; in part by the EU H2020 RISE TESTBED2 Project under Grant 872172; in part by the Taishan Scholar Program of Shandong Province; in part by the Shandong Provincial Natural Science Foundation under Grant ZR2020QF001 and Grant ZR2019BF04; and the Fundamental Research Funds of Shandong University under Grant 2020GN032. The associate editor coordinating the review of this article and approving it for publication was Z. Sun. *(Corresponding author: Cheng-Xiang Wang.)*

Ji Bian is with the School of Information Science and Engineering, Shandong Normal University, Jinan, Shandong 250358, China (e-mail: jibian@sdnu.edu.cn).

Cheng-Xiang Wang, Rui Feng, Wenqi Zhou, Fan Lai, and Xiqi Gao are with the National Mobile Communications Research Laboratory, School of Information Science and Engineering, Southeast University, Nanjing 210096, China, and also with the Purple Mountain Laboratories, Nanjing 211111, China (e-mail: chxwang@seu.edu.cn; fengxiurui604@163.com; wqzhou@seu.edu.cn; lai_fan@seu.edu.cn; xqgao@seu.edu.cn).

Yu Liu is with the School of Microelectronics, Shandong University, Jinan, Shandong 250101, China (e-mail: yuliu@sdu.edu.cn).

Color versions of one or more figures in this article are available at https://doi.org/10.1109/TWC.2022.3205929.

Digital Object Identifier 10.1109/TWC.2022.3205929

the array. Similarly, measurements in [12] were performed at 6 GHz using a 64-element virtual linear array. Results reveal that the multipath components (MPCs) of the massive MIMO channel are evolved over the array. The quasi-stationarity region in the array domain was estimated. Apart from sub-6 GHz, more meaningful results were obtained at mmWave bands [13], [14]. Measurement results show that mmWave massive MIMO channels are significantly array non-stationary. The birth-death processes associated with each cluster are correlated. The closer between two antennas, the more common scatterers they share. Compared with sub-6 GHz bands, mmWave massive MIMO channels illustrate more dramatic changes of cluster number across the array due to the significant scattering effect and high attenuation.

In general, the stochastic massive MIMO channel models can be divided into geometry-based stochastic models (GBSMs) and non-geometrical stochastic models (NGSMs), depending on whether the geometric distributions of scatterers are taken into account [10], [15], [16]. For massive MIMO GBSMs, the widely adopted approach is combining traditional GBSMs with array birth-death or Markov processes, which are used to simulate the non-stationary behavior of clusters over array [17], [18]. The model in [19] was designed by combining a twin-cluster model and a two-state Markov process. Similarly, the model in [20] was developed by extending a 3GPP/WINNER-like model with birth-death processes. Another method for massive MIMO channel modeling is introducing the concept of visibility region (VR) into array domain [21], [22]. The VR refers to a region on the large array and each cluster is assigned to a specific VR. Only when an antenna is in the VR, the corresponding cluster can be observed by the antenna.

Benefitting from the simple structure, NGSMs are often used in system performance evaluation. Different from the GBSMs, researches on massive MIMO NGSMs are in the preliminary phase. Most of the existing works were developed as classical correlation-based stochastic models (CBSMs), e.g., Kronecker models [23] and Weichselberger models [24]. Other massive MIMO NGSMs were designed as traditional BDCMs, e.g., [5], [6], [25], and [26]. By sampling the propagation environment in the angular domain, BDCMs characterize the power coupling between transmit and receive beams. As antenna number increases, beam domain channel elements tend to be uncorrelated and illustrate a frequency-flat property [6]. However, most of the existing BDCMs were developed based on the simple Saleh-Valenzuela (SV) model [5], [26], [27], [28] or spatial spreading function without considering the array non-stationarity [6], [25]. This makes those models not accurate enough and can lead to erroneous results about the performance of beam domain communication systems.

B. Motivations

A realistic and efficient BDCM plays a fundamental role in design and performance evaluation of beam domain massive MIMO systems. However, to the best of the authors knowledge, none of the existing BDCMs take the array non-stationarity into consideration, which has been shown to have great impacts on massive MIMO channel behaviors [14], [21]. Besides, in the existing massive MIMO channel models, the birth-death processes or the VRs associated with different clusters are modeled independently [19], [29]. However, measurements indicate that the array non-stationarities for different clusters are correlated. The smaller distance between two antennas, the more common clusters they can observe [12]. Furthermore, most of the existing massive MIMO channel models described the array non-stationarity in cluster level. This implies that the MPCs within a cluster experience the same birth-death process or have the same VR, which is inconsistent with the measurement results [14]. It is more reasonable to model the array non-stationarity in the MPC level. In sum, how to model the array non-stationarity realistically, how to incorporate array non-stationarity into the BDCM, and how does array non-stationarity affect the beam domain channel behaviors. These challenges have not been well addressed.

C. Contributions

In this paper, we propose a novel 3D BDCM by incorporating the array non-stationarity of massive MIMO channels. The impacts of array non-stationarity on beam domain channel statistics and system performance are analyzed. The main contributions are listed as follows:

1) A novel BDCM is proposed, which is the first BDCM incorporating the effects of array non-stationarity. We find that the beamwidths and spatial resolutions of the beam domain channel for different directions are not equal due to the array non-stationarity, which is different from the existing BDCMs. By adjusting model parameters, the proposed model can support various propagation scenarios and array configurations.
2) A new modeling method called spatially consistent cluster VR is proposed to describe the visibility of clusters over a large array considering the correlations among different clusters. Based on the cluster VRs, the array non-stationarity is depicted in terms of individual MPCs.
3) The impacts of array non-stationarity on beam domain channel statistics are firstly revealed, including beamwidth, channel power, power leakage, and space-time-frequency correlation function (STF-CF). The influences of array non-stationarity on ergodic capacity and outage capacity are also analyzed. Power dispersion of the beam domain channel is described by a novel statistic called beam spread, which is compared with angular spread and validated by measurements.

The rest of this paper is organized as follows. In Section II, the novel BDCM incorporating the array non-stationarity of massive MIMO channels is proposed. The statistical properties of the proposed BDCM are derived in Section III. Section IV extends the proposed BDCM for different array configurations. Results and analysis are given in Section V, and conclusions are drawn in Section VI.

Notation: $|\cdot|$ returns absolute value, $\|\cdot\|$ calculates length of a vector, $(\cdot)^*$, $(\cdot)^{\mathrm{T}}$, and $(\cdot)^{\mathrm{H}}$ denote complex conjugation, transpose, and conjugate transpose operations, respectively, $\lceil\cdot\rceil$

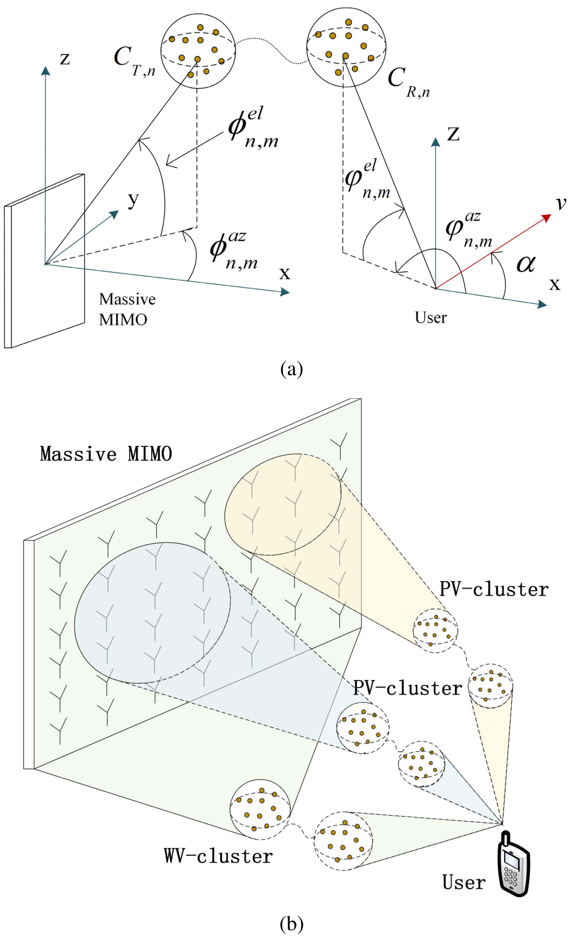

Fig. 1. Wideband massive MIMO communication systems. (a) Angular parameters of the massive MIMO channel, (b) Multi-bounce scattering propagation with WV-clusters and PV-clusters.

is the ceiling function, $\odot$ and $\otimes$ are the Schur-Hadamard product and Kronecker product, respectively, $\mathbb{E}(\cdot)$ accounts for statistical average, $\delta(\cdot)$ is the Kronecker delta function, $\mathrm{tr}(\cdot)$ denotes the trace operator, and $\det(\cdot)$ denotes determinant operation.

II. Novel Beam Domain Channel Model for Massive MIMO Systems

Fig. 1(a) shows the massive MIMO communication system where the BS employs a large uniform planar array (UPA) and communicates with a single-antenna UT. The BS is assumed to be fixed and the UT can move in horizontal plane with speed v and moving direction α. Without loss of generality, the large UPA is aligned on the y-z plane and has a dimension of $P = P_h \times P_v$, where P_h and P_v are the numbers of antenna elements in horizontal and vertical dimensions, respectively. Symbols d_h and d_v denote the horizontal and vertical spacings between adjacent elements, respectively. Considering a multi-bounce scattering propagation containing N clusters, each cluster can be described by the first-bounce cluster, i.e., $C_{T,n}$ and the last-bounce cluster, i.e., $C_{R,n}$. For clarity, only the nth cluster is shown in Fig. 1(a). The azimuth angles of departure (AAoDs), elevation AoDs (EAoDs), azimuth angles of arrival (AAoAs), and elevation AoAs (EAoAs) of the mth ($m = 1, \ldots, M_n$) path in the nth cluster is denoted by $\phi^{az}_{n,m}$, $\phi^{el}_{n,m}$, $\varphi^{az}_{n,m}$, and $\varphi^{el}_{n,m}$, respectively. The propagation between the first- and last-bounce clusters is not defined and considered as a virtual link [30]. Key parameters of the channel model are collected in Table I.

A. Novel GBSM for Massive MIMO Systems

Considering the large aperture size of the array, clusters in massive MIMO channels can be classified as wholly visible (WV)-clusters and partially visible (PV)-clusters, which are shown in Fig. 1(b). The WV-clusters are defined as clusters that can be observed by the whole array. The PV-clusters indicate clusters that can only be seen by part of the array. The PV-cluster percentage η is introduced to describe the proportion of PV-clusters in the whole clusters. For a certain number of antennas, a compact planar array can experience smaller array non-stationarity compared with a large linear array, and therefore resulting in a lower PV-cluster percentage [11]. Besides, it is found that the WV-clusters are caused by the reflections from dominant scatterers. However, the PV-clusters are more likely to be observed in rich scattering environments where MPCs experience complex scattering paths [14]. To reduce the portion of PV-clusters, compact antenna arrays should be used and the locations of BS and UT should be carefully chosen, hence more energy can be received via dominant scatterers. For simplicity of simulations, in this paper the PV-cluster indexes are randomly drawn from the whole cluster set following the uniform distribution. The channel transfer function corresponding to the antenna in the ith ($i = 1, \ldots, P_v$) row and the jth ($j = 1, \ldots, P_h$) column of the UPA, i.e., $A_{i,j}$, can be modeled as

$$h_{i,j}(t,f) = h^{\mathrm{WV}}_{i,j}(t,f) + h^{\mathrm{PV}}_{i,j}(t,f) \tag{1}$$

where $h^{\mathrm{WV}}_{i,j}(t,f)$ and $h^{\mathrm{PV}}_{i,j}(t,f)$ are the WV and PV components of the transfer function, respectively, and are given as

$$h^{\mathrm{WV}}_{i,j}(t,f) = \sum_{n\in\mathcal{B}_{\mathrm{WV}}} \sum_{m=1}^{M_n} \beta_{n,m} \cdot e^{j[2\pi(\nu_{n,m}t - f\tau_{n,m}) + \Phi_{n,m}]} \times e^{j\frac{2\pi}{\lambda}[(i-1)d_h \cos\phi^{el}_{n,m} \sin\phi^{az}_{n,m} + (j-1)d_v \sin\phi^{el}_{n,m}]} \tag{2}$$

$$h^{\mathrm{PV}}_{i,j}(t,f) = \sum_{n\in\mathcal{B}_{\mathrm{PV}}} \sum_{m=1}^{M_n} \beta_{n,m} \cdot \xi_{ij,nm} \cdot e^{j[2\pi(\nu_{n,m}t - f\tau_{n,m}) + \Phi_{n,m}]} \times e^{j\frac{2\pi}{\lambda}[(i-1)d_h \cos\phi^{el}_{n,m} \sin\phi^{az}_{n,m} + (j-1)d_v \sin\phi^{el}_{n,m}]} \tag{3}$$

where M_n is the number of paths in the nth cluster, λ stands for the wavelength, $\mathcal{B}_{\mathrm{WV}}$ and $\mathcal{B}_{\mathrm{PV}}$ denote index sets of WV- and PV-clusters, respectively. In (3), the partially visible property of each MPC is modeled by the path visibility factor $\xi_{ij,nm} \in \{0,1\}$, indicating whether the mth path in the nth cluster can be observed by the antenna $A_{i,j}$. Details on $\xi_{ij,nm}$ are described in Section II-B. Note that the line-of-sight (LoS) component can be viewed as a special WV-cluster containing one path. Therefore, the path gain of the LoS component can be defined as $\beta_{n,m} = \sqrt{\frac{K_R}{K_R+1}}$ where $n = 0$ and the path

TABLE I
SUMMARY OF KEY PARAMETER DEFINITIONS

$A_{i,j}$	Antenna in the ith row and the jth column of the UPA
P_h, P_v	Dimensions of the array in azimuth and elevation, respectively
P	Number of antennas in the large UPA
d_h, d_v	Spacings of adjacent antennas in azimuth and elevation, respectively
v, α	Speed and travel azimuth angle of the UT, respectively
$C_{T,n}$, $C_{R,n}$	The nth cluster at the BS and UT sides, respectively
N, M_n	Number of clusters and number of paths in the nth cluster, respectively
$\phi^{az}_{n,m}$, $\varphi^{az}_{n,m}$	Azimuth angles of the mth path in the nth cluster at the BS and UT sides, respectively
$\phi^{el}_{n,m}$, $\varphi^{el}_{n,m}$	Elevation angles of the mth path in the nth cluster at the BS and UT sides, respectively
$\mathcal{B}_{\text{WV}}$, $\mathcal{B}_{\text{PV}}$	WV- and PV-cluster index sets, respectively

gains of NLoS components are defined as $\beta_{n,m} = \sqrt{\frac{P_{n,m}}{K_R+1}}$ where $n = 1, \ldots, N$. Besides, K_R designates the Rice factor, $\tau_{n,m}$ and $P_{n,m}$ account for the delay and power of the mth path in the nth cluster, respectively. Furthermore, $\nu_{n,m} = f_m \cdot \cos\varphi^{el}_{n,m} \cos(\varphi^{az}_{n,m} - \alpha)$ is the Doppler frequency due to the movement of the UT, where $f_m = v/\lambda$. The phase shifts $\Phi_{n,m}$ are caused by the interactions between the waves and scatterers and modeled as i.i.d. random variable uniformly distributed over $[0, 2\pi)$.

In the proposed model, the MPC VR refers to a region on the large array which can be observed by the MPC. A cluster VR is defined as the union of VRs of the MPCs within the cluster. This implies that each MPC within a cluster can have its own evolution process, which is more consistent with the measurement results [13], [31]. For ease of analysis, the channel transfer function is written as a $P_v \times P_h$ matrix, i.e.,

$$\mathbf{H}(t, f) = \mathbf{H}^{\text{WV}}(t, f) + \mathbf{H}^{\text{PV}}(t, f) \tag{4}$$

with

$$\mathbf{H}^{\text{WV}}(t, f) = \sum_{n\in\mathcal{B}_{\text{WV}}} \sum_{m=1}^{M_n} \beta_{n,m} e^{j[2\pi(\nu_{n,m}t - f\tau_{n,m}) + \Phi_{n,m}]} \times \mathbf{U}(\theta^{az}_{n,m}, \theta^{el}_{n,m}) \tag{5}$$

$$\mathbf{H}^{\text{PV}}(t, f) = \sum_{n\in\mathcal{B}_{\text{PV}}} \sum_{m=1}^{M_n} \beta_{n,m} e^{j[2\pi(\nu_{n,m}t - f\tau_{n,m}) + \Phi_{n,m}]} \times \hat{\mathbf{U}}(\theta^{az}_{n,m}, \theta^{el}_{n,m}) \tag{6}$$

where $\mathbf{U}(\theta^{az}_{n,m}, \theta^{el}_{n,m}) \in \mathbb{C}^{P_v \times P_h}$ is the response matrix of the UPA, i.e.,

$$\mathbf{U}(\theta^{az}_{n,m}, \theta^{el}_{n,m}) = \begin{bmatrix} 1 & \cdots & e^{j2\pi(P_h-1)\theta^{az}_{n,m}} \\ e^{j2\pi\theta^{el}_{n,m}} & \cdots & e^{j2\pi[\theta^{el}_{n,m} + (P_h-1)\theta^{az}_{n,m}]} \\ \vdots & \ddots & \vdots \\ e^{j2\pi(P_v-1)\theta^{el}_{n,m}} & \cdots & e^{j2\pi[(P_v-1)\theta^{el}_{n,m} + (P_h-1)\theta^{az}_{n,m}]} \end{bmatrix} \tag{7}$$

where $\theta^{az}_{n,m} = d_h/\lambda \cos\phi^{el}_{n,m} \sin\phi^{az}_{n,m}$ and $\theta^{el}_{n,m} = d_v/\lambda \sin\phi^{el}_{n,m}$ are spatial frequencies in azimuth and elevation directions associated with the mth path in the nth cluster [32]. For the critically spaced arrays, i.e., $d_h = d_v = \lambda/2$, $\{\theta^{az}_j, \theta^{el}_i\} \in [-0.5, 0.5] \times [-0.5, 0.5]$. Furthermore, $\hat{\mathbf{U}}(\theta^{az}_{n,m}, \theta^{el}_{n,m})$ is the response matrix for the PV-MPCs, and can be obtained as

$$\hat{\mathbf{U}}(\theta^{az}_{n,m}, \theta^{el}_{n,m}) = \mathbf{U}(\theta^{az}_{n,m}, \theta^{el}_{n,m}) \odot \boldsymbol{\xi}_{n,m} \tag{8}$$

where $\boldsymbol{\xi}_{n,m}$ is the mask matrix composed of $\xi_{ij,nm}$ and defines the VR of the mth path in the nth cluster over the UPA.

B. VR Modeling in the Array Domain

In the proposed model, the VRs in the array domain are modeled in two stages. Firstly, the lengths and positions of the cluster VR in horizontal and vertical directions are generated. Then the VRs of MPCs within the cluster are determined, including their lengths and positions.

1) Cluster VR Length: The horizontal and vertical dimensions of the VR for the nth cluster in the UPA are defined as

$$\mathcal{L}^{h/v}_{C,n} = (I^{h/v}_{e,n} - I^{h/v}_{s,n}) \cdot d_{h/v} \tag{9}$$

where $I^h_{s,n}$ and $I^h_{e,n}$ stand for the start and end column indexes of the antenna elements in the cluster VR, respectively. Symbols $I^v_{s,n}$ and $I^v_{e,n}$ account for the start and end row indexes of the antenna elements in the cluster VR, respectively. In general, the channel non-stationarity in the array domain is not isotropic, which implies that the cluster VR lengths in horizontal and vertical directions are different, and can be modeled as independent random variables following exponential distribution, i.e., $\mathcal{L}^{h/v}_{C,n} \sim \text{Exp}(\lambda^{h/v}_C)$ [13].

2) Spatially Consistent Cluster VR Positions: Similar to other channel parameters, VR positions should be spatially consistent, which means two closely located clusters can have similar VRs [33]. Inspired by [34], the concept of cluster distance is introduced to measure the distance between two clusters. The distance between the kth and the lth clusters is calculated as

$$\text{CD}_{kl} = \sqrt{\|\text{CD}_{\phi,kl}\|^2 + \|\text{CD}_{\varphi,kl}\|^2 + \text{CD}^2_{\tau,kl}} \tag{10}$$

where

$$\text{CD}_{\phi/\varphi,kl} = \frac{1}{2}\left|\boldsymbol{\Omega}^{T/R}_k - \boldsymbol{\Omega}^{T/R}_l\right| \tag{11}$$

and $\boldsymbol{\Omega}^{T/R}_k$ are angle unit vectors of departure/arrival waves of the kth cluster, i.e.,

$$\boldsymbol{\Omega}^T_k = [\cos\phi^{el}_k \cos\phi^{az}_k, \cos\phi^{el}_k \sin\phi^{az}_k, \sin\phi^{el}_k]^{\text{T}} \tag{12}$$

$$\boldsymbol{\Omega}^R_k = [\cos\varphi^{el}_k \cos\varphi^{az}_k, \cos\varphi^{el}_k \sin\varphi^{az}_k, \sin\varphi^{el}_k]^{\text{T}} \tag{13}$$

where ϕ^{az}_k, ϕ^{el}_k, φ^{az}_k, and φ^{el}_k are the mean values of AAoDs, EAoDs, AAoAs, and EAoAs of MPCs within the cluster, respectively. Note that the value of $|\boldsymbol{\Omega}^{T/R}_k - \boldsymbol{\Omega}^{T/R}_l|$ represents the distance of two vectors on the unit sphere. The coefficient 1/2 ensures that $\|\mathrm{CD}_{\phi/\varphi,kl}\|$ is in the interval of $[0,1]$. The delay distance can be written as

$$\mathrm{CD}_{\tau,kl}=\frac{|\tau_k-\tau_l|}{\Delta\tau_{\max}}\cdot\frac{\tau_{\mathrm{std}}}{\Delta\tau_{\max}} \tag{14}$$

where τ_k denotes the delay of the kth cluster, $\Delta\tau_{\max}=\max(\tau_k)-\min(\tau_k)$, τ_{std} is standard deviation of cluster delays. The cluster distance can be viewed as the radius of a hypersphere in the normalized cluster parameter distance space. Based on $\mathrm{CD}_{k,l}$, spatially consistent VR positions can be generated using the exponential spatial filter method as follows [35]

$$\tilde{I}^{h/v}_{s,k}=\sum_{l\in\mathcal{B}_{\mathrm{PV}}}\hat{I}^{h/v}_{s,l}\cdot\rho(k,l). \tag{15}$$

Here, $\hat{I}^{h/v}_{s,l}$ and $I^{h/v}_{s,l}=\lceil\tilde{I}^{h/v}_{s,k}\rceil$ are the independent and correlated start column/row indexes of antennas, respectively, $\rho(k,l)$ is the exponential spatial filter, i.e.,

$$\rho'(k,l)=e^{-\frac{\mathrm{CD}_{k,l}}{\Delta_C}}. \tag{16}$$

Note that the spatial filter should be normalized as $\rho(k,l)=\frac{\rho'(k,l)}{\sum_{l\in\mathcal{B}_{\mathrm{PV}}}\rho'(k,l)}$. Parameter Δ_C is the cluster correlation factor controlling the shape of the filter. In general, $\hat{I}^{h}_{s,l}$ and $\hat{I}^{v}_{s,l}$ follow uniform distributions in horizontal and vertical directions within the UPA, respectively.

3) VR of MPCs Within the Cluster: Since the dimensions of cluster VR have been modeled, the dimensions of MPC VR are defined with respect to the cluster VR, i.e.,

$$\mathcal{L}^{h/v}_{M,nm}=\frac{(I^{h/v}_{e,nm}-I^{h/v}_{s,nm})\cdot d_{h/v}}{\mathcal{L}^{h/v}_{C,n}} \tag{17}$$

where $I^{h/v}_{s,nm}$ and $I^{h/v}_{e,nm}$ are the start and end column/row indexes for the mth path in the nth cluster, respectively. According to the channel measurements in [14], the horizontal and vertical lengths of the MPC VR within a cluster are modeled by the exponential distribution with the rate parameter $\lambda^{h/v}_{M}$. Furthermore, positions of MPC VRs in horizontal and vertical directions are found to be uniformly distributed within the cluster VR.

C. Novel BDCM for Massive MIMO Systems

For ease of analysis, the channel transfer function in (4) is rearranged as a $1\times P$ matrix,

$$\mathbf{H}(t,f)=\mathbf{H}^{\mathrm{WV}}(t,f)+\mathbf{H}^{\mathrm{PV}}(t,f) \tag{18}$$

with

$$\mathbf{H}^{\mathrm{WV}}(t,f)=\sum_{n\in\mathcal{B}_{\mathrm{WV}}}\sum_{m=1}^{M_n}\beta_{n,m}e^{j[2\pi(\nu_{n,m}t-f\tau_{n,m})+\Phi_{n,m}]}\times[\mathbf{b}(\theta^{el}_{n,m})\otimes\mathbf{a}(\theta^{az}_{n,m})]^{\mathrm{T}} \tag{19}$$

$$\mathbf{H}^{\mathrm{PV}}(t,f)=\sum_{n\in\mathcal{B}_{\mathrm{PV}}}\sum_{m=1}^{M_n}\beta_{n,m}e^{j[2\pi(\nu_{n,m}t-f\tau_{n,m})+\Phi_{n,m}]}\times[\hat{\mathbf{b}}(\theta^{el}_{n,m})\otimes\hat{\mathbf{a}}(\theta^{az}_{n,m})]^{\mathrm{T}} \tag{20}$$

where $\mathbf{a}(\theta^{az}_{n,m})$ and $\mathbf{b}(\theta^{el}_{n,m})$ are response vectors of in azimuth and elevation for the WV-MPCs, respectively, i.e.,

$$\mathbf{a}(\theta^{az}_{n,m})=[1,e^{j2\pi\theta^{az}_{n,m}},\ldots,e^{j2\pi(P_h-1)\theta^{az}_{n,m}}]^{\mathrm{T}} \tag{21}$$

$$\mathbf{b}(\theta^{el}_{n,m})=[1,e^{j2\pi\theta^{el}_{n,m}},\ldots,e^{j2\pi(P_v-1)\theta^{el}_{n,m}}]^{\mathrm{T}}. \tag{22}$$

Furthermore, $\hat{\mathbf{a}}(\theta^{az}_{n,m})$ and $\hat{\mathbf{b}}(\theta^{el}_{n,m})$ are the response vectors for the PV-MPCs, and given as

$$\hat{\mathbf{a}}(\theta^{az}_{n,m})=[\mathbf{O}_{I^h_{s,nm}-1},e^{j2\pi(I^h_{s,nm}-1)\theta^{az}_{n,m}},\ldots,\times e^{j2\pi(I^h_{e,nm}-1)\theta^{az}_{n,m}},\mathbf{O}_{P_h-I^h_{e,nm}}]^{\mathrm{T}} \tag{23}$$

$$\hat{\mathbf{b}}(\theta^{el}_{n,m})=[\mathbf{O}_{I^v_{s,nm}-1},e^{j2\pi(I^v_{s,nm}-1)\theta^{el}_{n,m}},\ldots,\times e^{j2\pi(I^v_{e,nm}-1)\theta^{el}_{n,m}},\mathbf{O}_{P_v-I^v_{e,nm}}]^{\mathrm{T}} \tag{24}$$

where $\mathbf{O}_n$ stands for a row vector with n zeros entries. The BDCM is generated based on the proposed GBSM through a discrete Fourier transform (DFT)-based beamforming operation as follows [6]

$$\mathbf{H}_B(t,f)=\mathbf{H}(t,f)\tilde{\mathbf{U}}^{*} \tag{25}$$

where $\tilde{\mathbf{U}}\in\mathbb{C}^{P\times P}$ is the transmit beamforming matrix and defined as

$$\tilde{\mathbf{U}}=\tilde{\mathbf{U}}_{el}\otimes\tilde{\mathbf{U}}_{az} \tag{26}$$

where

$$\tilde{\mathbf{U}}_{az}=\frac{1}{\sqrt{P_h}}[\mathbf{a}(\tilde{\theta}^{az}_{j})]_{j=1,\ldots,P_h}\in\mathbb{C}^{P_h\times P_h} \tag{27}$$

$$\tilde{\mathbf{U}}_{el}=\frac{1}{\sqrt{P_v}}[\mathbf{b}(\tilde{\theta}^{el}_{i})]_{i=1,\ldots,P_v}\in\mathbb{C}^{P_v\times P_v}. \tag{28}$$

The columns of $\tilde{\mathbf{U}}_{az}$ and $\tilde{\mathbf{U}}_{el}$ are response vectors associated with P_h and P_v uniformly spaced spatial frequencies, respectively, i.e., $\tilde{\theta}^{az}_{j}=\frac{2j-1}{2P_h}-0.5$ and $\tilde{\theta}^{el}_{i}=\frac{2i-1}{2P_v}-0.5$. Since the Kronecker product of two unitary matrices is still unitary, $\mathbf{H}(t,f)$ and $\mathbf{H}_B(t,f)$ are unitary equivalence. By substituting (18) into (25), the beam domain channel matrix considering WV- and PV-clusters can be further expressed as

$$\mathbf{H}_B(t,f)=\mathbf{H}^{\mathrm{WV}}_B(t,f)+\mathbf{H}^{\mathrm{PV}}_B(t,f) \tag{29}$$

where $\mathbf{H}^{\mathrm{WV}}_B(t,f)$ and $\mathbf{H}^{\mathrm{PV}}_B(t,f)$ are the WV and PV components of BDCM. The channel element corresponding to the jth AAoD and the ith EAoD is given as

$$h_{B,ij}(t,f)=h^{\mathrm{WV}}_{B,ij}(t,f)+h^{\mathrm{PV}}_{B,ij}(t,f) \tag{30}$$

with

$$h^{\mathrm{WV}}_{B,ij}(t,f)=\frac{1}{\sqrt{P}}\sum_{n\in\mathcal{B}_{\mathrm{WV}}}\sum_{m=1}^{M_n}\beta_{n,m}\cdot e^{j[2\pi(\nu_{n,m}t-f\tau_{n,m})+\Phi_{n,m}]}f_{1,P_v}(\theta^{el}_{n,m}-\tilde{\theta}^{el}_{i})\cdot f_{1,P_h}(\theta^{az}_{n,m}-\tilde{\theta}^{az}_{j}) \tag{31}$$

$$h^{\mathrm{PV}}_{B,ij}(t,f)=\frac{1}{\sqrt{P}}\sum_{n\in\mathcal{B}_{\mathrm{PV}}}\sum_{m=1}^{M_n}\beta_{n,m}\cdot e^{j[2\pi(\nu_{n,m}t-f\tau_{n,m})+\Phi_{n,m}]}f_{I^v_{s,nm},I^v_{e,nm}}(\theta^{el}_{n,m}-\tilde{\theta}^{el}_{i})\cdot f_{I^h_{s,nm},I^h_{e,nm}}(\theta^{az}_{n,m}-\tilde{\theta}^{az}_{j}) \tag{32}$$

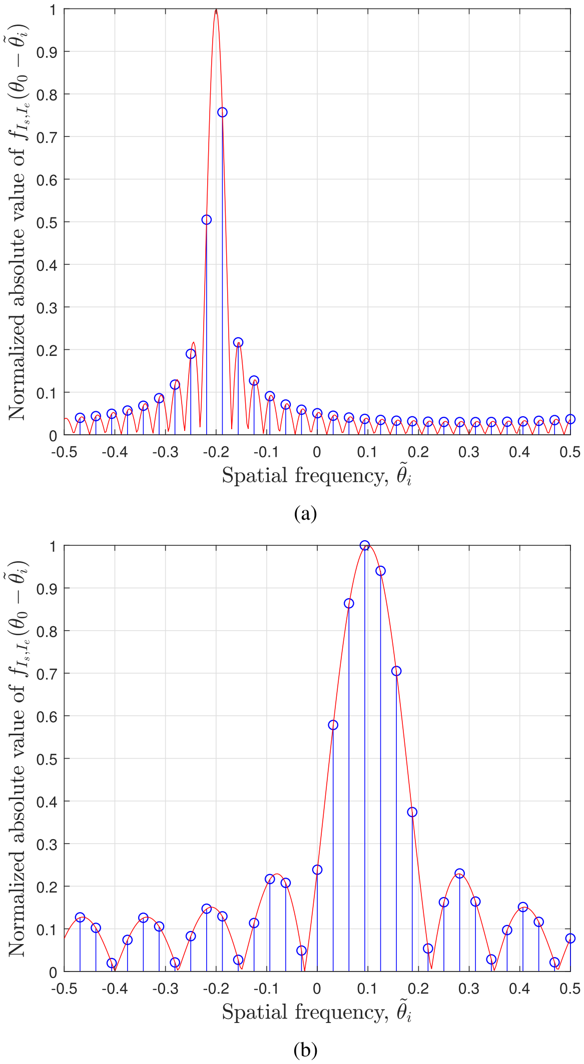

Fig. 2. Normalized absolute values of $f_{I_s,I_e}(\theta_0-\tilde{\theta}_j)$ for (a) a WV-MPC with $\theta_0 = -0.2$ and (b) a PV-MPC with $\theta_0 = 0.1$ ($P_h = 32$, $\tilde{\theta}_j = \frac{2j-1}{2P_h} - 0.5, j = 1,\ldots,P_h$, $I_e - I_s = 7$).

where

$$f_{I_s,I_e}(x) = e^{j\pi x(I_s+I_e-2)} \frac{\sin[\pi x(I_e - I_s + 1)]}{\sin(\pi x)}. \quad (33)$$

The derivations of (31) and (32) are given in the Appendix-A.

Fig. 2 shows the normalized absolute values of $f_{I_s,I_e}(\theta_0 - \tilde{\theta}_j)$ for a WV-MPC and a PV-MPC in azimuth where $P_h = 32$. The WV-MPC can be observed by the whole 32 antennas and the VR of the PV-MPC covers 8 consecutive antennas. In the two cases, $f_{I_s,I_e}(\theta_0 - \tilde{\theta})$ are uniformly sampled at directions $\tilde{\theta}_j$ ($j = 1,\ldots,P_h$) and are peaky around θ_0. Compared to the WV-MPC case, the beamwidth for the PV-MPC is wider due to the partially visible property. The beamwidth associated with the VR length can be measured as $\Delta\theta = \frac{1}{I_e - I_s + 1}$, which is inversely proportional to the VR length of the MPC. Note that $f_{I_s,I_e}(x)$ is zero when x is an integral multiple of $\Delta\theta$. By setting $I_s = 1$, $I_e = P_h$, the beamwidth for the WV-MPC case becomes $\frac{1}{P_h}$. This indicates that in massive MIMO beam domain channels, the beamwidths or spatial resolutions for different directions may not exactly equal due to the partially visible property of PV-MPCs. The WV-MPCs lead to the narrowest beams and a shorter VR of PV-MPC results in a wider beamwidth.

III. Characteristics of the Proposed BDCM

A. Channel Power

The power of the beam domain channel can be calculated as

$$\mathbb{E}\{\mathrm{tr}(\mathbf{H}_B^{\mathrm{H}}\mathbf{H}_B)\} = \sum_{i=1}^{P_h}\sum_{j=1}^{P_v} \mathbb{E}\left\{\left|h_{B,ij}\right|^2\right\}. \quad (34)$$

Based on (30)–(32) and uncorrelated scattering assumption, the power of the channel elements can be written as

$$\mathbb{E}\left\{\left|h_{B,ij}\right|^2\right\} = \Omega_{i,j}^{\mathrm{WV}} + \Omega_{i,j}^{\mathrm{PV}} \quad (35)$$

with

$$\begin{aligned}\Omega_{i,j}^{\mathrm{WV}} &= \frac{1}{P}\sum_{n\in\mathcal{B}_{\mathrm{WV}}}\sum_{m=1}^{M_n} \beta_{n,m}^2 \left|D_{P_h}(\theta_{n,m}^{az} - \tilde{\theta}_j^{az})\right|^2 \\ &\quad \times \left|D_{P_v}(\theta_{n,m}^{el} - \tilde{\theta}_i^{el})\right|^2 \quad (36)\\ \Omega_{i,j}^{\mathrm{PV}} &= \frac{1}{P}\sum_{n\in\mathcal{B}_{\mathrm{PV}}}\sum_{m=1}^{M_n} \beta_{n,m}^2 \left|D_{I_{e,nm}^h - I_{s,nm}^h + 1}(\theta_{n,m}^{az} - \tilde{\theta}_j^{az})\right|^2 \\ &\quad \times \left|D_{I_{e,nm}^v - I_{s,nm}^v + 1}(\theta_{n,m}^{el} - \tilde{\theta}_i^{el})\right|^2 \quad (37)\end{aligned}$$

where $D_n(x) = \frac{\sin(\pi n x)}{\sin(\pi x)}$ denotes Dirichlet sinc function of degree n. As the dimensions of the array increase, $D_{P_h}(\theta_{n,m}^{az} - \tilde{\theta}_j^{az})$ and $D_{P_v}(\theta_{n,m}^{el} - \tilde{\theta}_i^{el})$ become peaky around the physical angles $\theta_{n,m}^{az}$ and $\theta_{n,m}^{el}$, respectively. Thus, we have the following approximations

$$\Omega_{i,j}^{\mathrm{WV}} \approx P \sum_{n\in\mathcal{B}_{\mathrm{WV}}}\sum_{m=1}^{M_n} \beta_{n,m}^2 \delta(\theta_{n,m}^{az} - \tilde{\theta}_j^{az}) \cdot \delta(\theta_{n,m}^{el} - \tilde{\theta}_i^{el}). \quad (38)$$

For the WV components, each WV-MPCs can be resolved in azimuth and elevation directions due to the large spatial resolution of the array. The power of each channel element corresponds to the power of the WV-MPC associated with a specific direction defined by $(\theta_{n,m}^{el}, \theta_{n,m}^{az})$. Therefore, multipath fading vanishes and the power leakage can be neglected. However, for the channel power contributed from the PV-MPCs, i.e., $\Omega_{i,j}^{\mathrm{PV}}$, the above approximated cannot hold because of the short VR lengths, which decrease the spatial resolution and introduce multipath fading for the beam domain channel.

B. Power Leakage

As is shown in Fig. 3(a), the power leakage refers to the fact that the power of a path spreads over a range of beam directions. In the traditional BDCM, the power leakage is caused by the mismatch between physical path angles and the spatial frequency sampling points [36], [37]. However, previous researches neglected the effects of partially visible property of MPCs, making the results not accurate enough

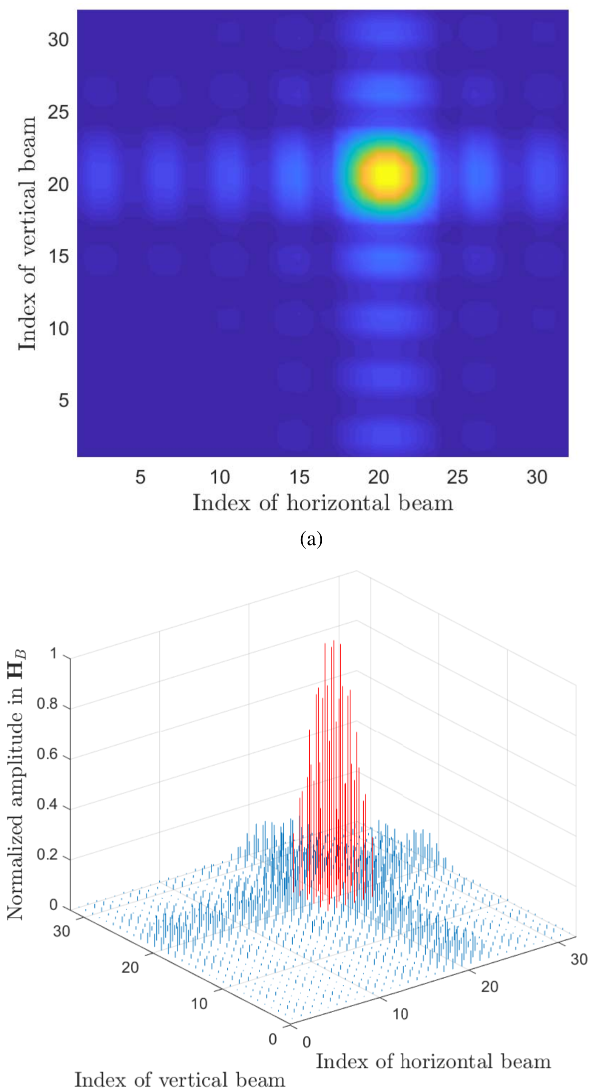

(a)

(b)

Fig. 3. Illustrations of the power leakage for a 32×32 UPA considering a single PV-MPC. (a) Beam pattern of the UPA. (b) Normalized amplitude distribution of the beam domain channel elements ($K_h = K_v = 6$, $I_e^{h(v)} - I_s^{h(v)} = 7$, $\theta_0^{el} = 4.5/P_v$, $\theta_0^{az} = 4.5/P_h$).

when evaluating massive MIMO systems. The power leakage for a PV-MPC can be defined as

$$\Gamma = 1 - \frac{\sum_{j \in \mathcal{U}(\theta_0^{az}, K_h), i \in \mathcal{U}(\theta_0^{el}, K_v)} \left|h_{B,ij}^{\mathrm{PV}}\right|^2}{\sum_{i,j=1}^{P_h, P_v} \left|h_{B,ij}^{\mathrm{PV}}\right|^2} \tag{39}$$

where, $\mathcal{U}(\theta_0^{az}, K_h)$ and $\mathcal{U}(\theta_0^{el}, K_v)$ are column and row index sets for a $K_v \times K_h$ submatrix centering around the physical direction of the MPC, i.e., $(\theta_0^{el}, \theta_0^{az})$. Therefore, the power leakage in (39) is actually measured by calculating the ratio of the power of the $K_v \times K_h$ submatrix around the main lobe direction to the total channel power. For clarity, Fig. 3(b) shows the amplitude distribution of channel elements for a 32×32 UPA. The red lines indicate the amplitudes of 6×6 channel elements around the direction $(\theta_0^{el}, \theta_0^{az})$. The power leakage stems from the rest of nonzero elements illustrated by blue lines. By substituting (32) into (39), we have

$$\Gamma = 1 - \frac{4\sum_{i=0}^{K_h/2-1} D^2_{I_e^h - I_s^h + 1}\left(\frac{2j+1}{2P_h}\right) \cdot \sum_{j=0}^{K_v/2-1} D^2_{I_e^v - I_s^v + 1}\left(\frac{2i+1}{2P_v}\right)}{(I_e^h - I_s^h + 1)(I_e^v - I_s^v + 1)P}. \tag{40}$$

The derivation of (40) is given in Appendix-B. By imposing $I_s^h = I_s^v = 1$, $I_e^h = P_h$, and $I_e^v = P_v$, the power leakage for a WV-MPC is obtained as

$$\Gamma = 1 - \frac{4}{P^2} \sum_{j=0}^{K_h/2-1} \sin\left(\frac{(2j+1)\pi}{2P_h}\right)^{-2} \cdot \sum_{i=0}^{K_v/2-1} \sin\left(\frac{(2i+1)\pi}{2P_v}\right)^{-2}. \tag{41}$$

C. STF-CF

The STF-CF between $h_{B,ij}(t,f)$ and $h_{B,i'j'}^*(t+\Delta t, f+\Delta f)$ is defined as

$$\gamma_{ij,i'j'}(\Delta t, \Delta f) = \mathbb{E}\left\{h_{B,ij}(t,f) h_{B,i'j'}^*(t+\Delta t, f+\Delta f)\right\}. \tag{42}$$

Here, Δt and Δf are time and frequency differences, respectively. Subscript $(\cdot)_{ij,i'j'}$ indicates the two transmit antennas A_{ij} and $A_{i'j'}$ separated by horizontal distance $\Delta j \cdot d_h$ and vertical distance $\Delta i \cdot d_v$, where $\Delta i = i' - i$ and $\Delta j = j' - j$. The STF-CF can be further written as the summation of PV and WV components, i.e. $\gamma_{ij,i'j'}(\Delta t, \Delta f) = \gamma_{ij,i'j'}^{\mathrm{WV}}(\Delta t, \Delta f) + \gamma_{ij,i'j'}^{\mathrm{PV}}(\Delta t, \Delta f)$. By substituting (31) and (32) into (42), the PV and WV components of STF-CF can be further expressed as

$$\begin{aligned}
&\gamma_{ij,i'j'}^{\mathrm{WV}}(\Delta t, \Delta f) \\
&\quad = \frac{1}{P} \sum_{n \in \mathcal{B}_{\mathrm{WV}}} \sum_{m=1}^{M_n} \beta_{n,m}^2 \cdot e^{j2\pi(\Delta f \tau_{n,m} - \nu_{n,m}\Delta t)} \\
&\qquad \times e^{j\pi\frac{(P_v-1)\Delta i}{P_v}} \cdot e^{j\pi\frac{(P_h-1)\Delta j}{P_h}} D_{P_v}(\theta_{n,m}^{el} - \tilde{\theta}_i^{el}) D_{P_v} \\
&\qquad \times (\theta_{n,m}^{el} - \tilde{\theta}_{i'}^{el}) D_{P_h}(\theta_{n,m}^{az} - \tilde{\theta}_j^{az}) D_{P_h}(\theta_{n,m}^{az} - \tilde{\theta}_{j'}^{az})
\end{aligned} \tag{43}$$

$$\begin{aligned}
&\gamma_{ij,i'j'}^{\mathrm{PV}}(\Delta t, \Delta f) \\
&\quad = \frac{1}{P} \sum_{n \in \mathcal{B}_{\mathrm{PV}}} \sum_{m=1}^{M_n} \beta_{n,m}^2 \cdot e^{j2\pi(\Delta f \tau_{n,m} - \nu_{n,m}\Delta t)} \\
&\qquad \times e^{j\pi(I_{s,nm}^v + I_{e,nm}^v - 2)\frac{\Delta i}{P_v}} \cdot e^{j\pi(I_{s,nm}^h + I_{e,nm}^h - 2)\frac{\Delta j}{P_h}} \\
&\qquad \times D_{I_{e,nm}^v - I_{s,nm}^v + 1}(\theta_{n,m}^{el} - \tilde{\theta}_i^{el}) D_{I_{e,nm}^v - I_{s,nm}^v + 1}(\theta_{n,m}^{el} \\
&\qquad \times - \tilde{\theta}_{i'}^{el}) D_{I_{e,nm}^h - I_{s,nm}^h + 1}(\theta_{n,m}^{az} - \tilde{\theta}_j^{az}) \\
&\qquad \times D_{I_{e,nm}^h - I_{s,nm}^h + 1}(\theta_{n,m}^{az} - \tilde{\theta}_{j'}^{az}).
\end{aligned} \tag{44}$$

Analogously, the STF-CF of the GBSM can be obtained as $\zeta_{ij,i'j'}(\Delta t, \Delta f) = \zeta_{ij,i'j'}^{\mathrm{WV}}(\Delta t, \Delta f) + \zeta_{ij,i'j'}^{\mathrm{PV}}(\Delta t, \Delta f)$, with

$$\begin{aligned}
\zeta_{ij,i'j'}^{\mathrm{WV}}(\Delta t, \Delta f) = &\sum_{n \in \mathcal{B}_{\mathrm{WV}}} \sum_{m=1}^{M_n} \beta_{n,m}^2 \cdot e^{j2\pi(\Delta f \tau_{n,m} - \nu_{n,m}\Delta t)} \\
&\times e^{-j\frac{2\pi}{\lambda}[\Delta j \cdot d_h \cos\phi_{n,m}^{el} \sin\phi_{n,m}^{az} + \Delta i \cdot d_v \sin\phi_{n,m}^{el}]}
\end{aligned} \tag{45}$$

$$\zeta^{\mathrm{PV}}_{ij,i'j'}(\Delta t,\Delta f)=\sum_{n\in\mathcal{B}_{\mathrm{PV}}}\sum_{m=1}^{M_n}\tilde{\beta}^2_{n,m}\cdot e^{j2\pi(\Delta f\tau_{n,m}-\nu_{n,m}\Delta t)}\times e^{-j\frac{2\pi}{\lambda}[\Delta j\cdot d_h\cos\phi^{el}_{n,m}\sin\phi^{az}_{n,m}+\Delta i\cdot d_v\sin\phi^{el}_{n,m}]} \tag{46}$$

where $\tilde{\beta}^2_{n,m}=\beta^2_{n,m}\cdot\xi_{ij,nm}\cdot\xi_{i'j',nm}$, which implies that only when the path is visible to $A_{i,j}$ and $A_{i',j'}$, it can contribute to the STF-CF. According to the definition in (25), the STF-CFs of the proposed GBSM and BDCM are related as $\mathbf{R}_B=\tilde{\mathbf{U}}^{\mathrm{H}}\mathbf{R}_G\tilde{\mathbf{U}}$, where $\mathbf{R}_B=\mathbb{E}\{\mathbf{H}_B^{\mathrm{T}}\mathbf{H}_B^*\}$ and $\mathbf{R}_G=\mathbb{E}\{\mathbf{H}_G^{\mathrm{T}}\mathbf{H}_G^*\}$ are $P\times P$ correlation matrices of the BDCM and GBSM, respectively. Considering the large aperture size of the UPA, $\gamma^{\mathrm{WV}}_{ij,i'j'}(\Delta t,\Delta f)$ can be approximated as

$$\gamma^{\mathrm{WV}}_{ij,i'j'}(\Delta t,\Delta f)\approx\sum_{n\in\mathcal{B}_{\mathrm{WV}}}\sum_{m=1}^{M_n}\beta^2_{n,m}\times\cdot e^{j2\pi(\Delta f\tau_{n,m}-\nu_{n,m}\Delta t)}\times\delta(\theta^{el}_{n,m}-\tilde{\theta}^{el}_i)\delta(\theta^{az}_{n,m}-\tilde{\theta}^{az}_j)\delta(\theta^{el}_{n,m}-\tilde{\theta}^{el}_{i'})\delta(\theta^{az}_{n,m}-\tilde{\theta}^{az}_{j'}). \tag{47}$$

The above approximation shows that the beam domain channel elements converted from WV-MPCs are approximately uncorrelated. On the contrary, the beam domain channel elements converted from PV-MPCs are correlated with each other due to the wide beamwidths. This indicates that the traditional BDCMs neglecting the array non-stationarity may underestimate correlation among beam domain channel elements.

D. RMS Beam Spread

The beam spread describes the power dispersion of the beam domain channel over different beam directions. Similar to the angular spread, the root mean square (RMS) azimuth beam spread can be defined as

$$\sigma^{\mathrm{az}}_B=\sqrt{\frac{\sum_{i,j=1}^{P_h,P_v}|h_{B,ij}|^2(\tilde{\phi}^{\mathrm{az}}_j-\mu^{\mathrm{az}})^2}{\sum_{i,j=1}^{P_h,P_v}|h_{B,ij}|^2}} \tag{48}$$

where μ^{az} is mean value of sampling azimuth angle $\tilde{\phi}^{\mathrm{az}}_j$ and can be calculated as the ratio of summation of the power-weighted azimuth angles to the total channel power, i.e.,

$$\mu^{\mathrm{az}}=\frac{\sum_{i,j=1}^{P_h,P_v}|h_{B,ij}|^2\tilde{\phi}^{\mathrm{az}}_j}{\sum_{i,j=1}^{P_h,P_v}|h_{B,ij}|^2}. \tag{49}$$

The elevation beam spread σ^{el}_B can be obtained by replacing $\tilde{\phi}^{\mathrm{az}}_j$ and μ^{az} with $\tilde{\phi}^{\mathrm{el}}_i$ and μ^{el} in (48) and (49), respectively. The sampling azimuth and elevation angles, i.e., $\tilde{\phi}^{\mathrm{az}}_j$ and $\tilde{\phi}^{\mathrm{el}}_i$, are determined according to the spatial frequencies as $\tilde{\theta}^{az}_j=d_h/\lambda\cos\tilde{\phi}^{el}_i\sin\tilde{\phi}^{az}_j$ and $\tilde{\theta}^{el}_i=d_v/\lambda\sin\tilde{\phi}^{el}_i$. A large beam spread means a large energy dispersion of the beam domain channel, which usually corresponds to a rich scattering environment. Both the angular spread and beam spread can depict the multipath richness of the channel. Note that the angular spreads are independent of array and only depend on the powers and angles of MPCs. However, the powers of beams are affected by the power leakage problem due to limited spatial resolution and array non-stationarity. The sampling angles $\tilde{\phi}^{\mathrm{az}}_j$ and $\tilde{\phi}^{\mathrm{el}}_i$ are also affected by the antenna numbers of the array. These make the beam spread array-dependent.

E. Channel Capacity

The spectral efficiency (in bit/s/Hz) for the proposed BDCM, considering channel knowledge at the Rx and is not available at the Tx, is calculated as [38]

$$C(x)=\frac{1}{N_f}\sum_{i=1}^{N_f}\log_2\left\{\det\left(\mathbf{I}_Q+\frac{\rho}{P}\mathbf{H}_{B,f_i}(x)\mathbf{H}^{\mathrm{H}}_{B,f_i}(x)\right)\right\} \tag{50}$$

where $\mathbf{H}_{B,f_i}(x)$ stands for the xth realization of the beam domain channel matrix at frequency f_i, N_f is the number of frequency points with bandwidth W, $\mathbf{I}_Q$ is $Q\times Q$ identity matrix, ρ is average signal-to-noise ratio (SNR). Here, the ergodic and outage capacities are adopted as the capacity metrics. The ergodic capacity, i.e., $C_{\mathrm{erg}}=\mathbb{E}\{C(x)\}$, is obtained as the statistical average of $C(x)$ over N_x individual channel realizations. The outage capacity C_{out} indicates the capacity where the cumulative distribution function (CDF) of $C(x)$ equals to the outage probability P_{out}.

IV. Extension for Different Array Configurations

A. UPAs at Both Ends

Considering both the Tx and Rx are equipped with large UPAs, the channel matrices in (19) and (20) are rewritten as $Q\times P$ matrices

$$\mathbf{H}^{\mathrm{WV}}(t,f)=\sum_{n\in\mathcal{B}_{\mathrm{WV}}}\sum_{m=1}^{M_n}\beta_{n,m}e^{j[2\pi(\nu_{n,m}t-f\tau_{n,m})+\Phi_{n,m}]}\times[\mathbf{b}_R(\vartheta^{el}_{n,m})\otimes\mathbf{a}_R(\vartheta^{az}_{n,m})][\mathbf{b}_T(\theta^{el}_{n,m})\otimes\mathbf{a}_T(\theta^{az}_{n,m})]^{\mathrm{T}} \tag{51}$$

$$\mathbf{H}^{\mathrm{PV}}(t,f)=\sum_{n\in\mathcal{B}_{\mathrm{PV}}}\sum_{m=1}^{M_n}\beta_{n,m}e^{j[2\pi(\nu_{n,m}t-f\tau_{n,m})+\Phi_{n,m}]}\times[\hat{\mathbf{b}}_R(\vartheta^{el}_{n,m})\otimes\hat{\mathbf{a}}_R(\vartheta^{az}_{n,m})][\hat{\mathbf{b}}_T(\theta^{el}_{n,m})\otimes\hat{\mathbf{a}}_T(\theta^{az}_{n,m})]^{\mathrm{T}} \tag{52}$$

where $\vartheta^{az}_{n,m}=0.5\cos\varphi^{el}_{n,m}\sin\varphi^{az}_{n,m}$ and $\vartheta^{el}_{n,m}=0.5\sin\varphi^{el}_{n,m}$. Besides, $Q=Q_h\times Q_v$, where Q_h and Q_v are the dimensions of Rx array in azimuth and elevation, respectively. The response vectors of the Rx array for the PV-MPCs, i.e, $\hat{\mathbf{a}}_R(\vartheta^{\mathrm{az}}_{n,m})$ and $\hat{\mathbf{b}}_R(\vartheta^{\mathrm{el}}_{n,m})$, are generated following the same procedure as discussed in Section II-B. The beam domain channel matrix can be obtained as [6]

$$\mathbf{H}_B(t,f)=\tilde{\mathbf{V}}^{\mathrm{H}}\mathbf{H}(t,f)\tilde{\mathbf{U}}^*. \tag{53}$$

Here, $\tilde{\mathbf{V}}\in\mathbb{C}^{Q\times Q}$ is the receive beamforming matrix and obtained as $\tilde{\mathbf{V}}=\tilde{\mathbf{V}}_{el}\otimes\tilde{\mathbf{V}}_{az}$, where $\tilde{\mathbf{V}}_{az}=\frac{1}{\sqrt{Q_h}}[\mathbf{a}(\tilde{\vartheta}^{az}_l)]_{l=1,\ldots,Q_h}$ and $\tilde{\mathbf{V}}_{el}=\frac{1}{\sqrt{Q_v}}[\mathbf{b}(\tilde{\vartheta}^{el}_k)]_{k=1,\ldots,Q_v}$. Furthermore, $\tilde{\vartheta}^{az}_l=\frac{2l-1}{2Q_h}-0.5$ and $\tilde{\vartheta}^{el}_k=\frac{2k-1}{2Q_v}-0.5$ are uniformly spaced spatial frequencies at the Rx side. The beam domain channel elements in (53) depict the coupling between transmit and receive beams. The elements in $\mathbf{H}_B^{\mathrm{WV}}(t,f)$ corresponding to the coupling between the beam with jth AAoD and ith EAoD, and the beam with lth AAoA and kth EAoA are expressed as

$$\begin{aligned} &h_{B,ij,kl}^{\mathrm{WV}}(t,f) \\ &\quad= \frac{1}{\sqrt{PQ}} \sum_{n\in\mathcal{B}_{\mathrm{WV}}} \sum_{m=1}^{M_n} \beta_{n,m}\cdot e^{j[2\pi(\nu_{n,m}t - f\tau_{n,m})+\Phi_{n,m}]} \\ &\qquad\times f_{1,P_v}(\theta_{n,m}^{el}-\tilde{\theta}_i^{el})\cdot f_{1,P_h}(\theta_{n,m}^{az}-\tilde{\theta}_j^{az}) \\ &\qquad\times f_{1,Q_v}(\vartheta_{n,m}^{el}-\tilde{\vartheta}_k^{el})\cdot f_{1,Q_h}(\vartheta_{n,m}^{az}-\tilde{\vartheta}_l^{az}). \end{aligned} \tag{54}$$

Analogously, the elements in $\mathbf{H}_B^{\mathrm{PV}}(t,f)$ are extended as

$$\begin{aligned} &h_{B,ij,kl}^{\mathrm{PV}}(t,f) \\ &\quad= \frac{1}{\sqrt{PQ}} \sum_{n\in\mathcal{B}_{\mathrm{PV}}} \sum_{m=1}^{M_n} \beta_{n,m}\cdot e^{j[2\pi(\nu_{n,m}t - f\tau_{n,m})+\Phi_{n,m}]} \\ &\qquad\times f_{I_{s,nm}^v,I_{e,nm}^v}(\theta_{n,m}^{el}-\tilde{\theta}_i^{el})\cdot f_{I_{s,nm}^h,I_{e,nm}^h}(\theta_{n,m}^{az}-\tilde{\theta}_j^{az}) \\ &\qquad\times f_{J_{s,nm}^v,J_{e,nm}^v}(\vartheta_{n,m}^{el}-\tilde{\vartheta}_k^{el})\cdot f_{J_{s,nm}^h,J_{e,nm}^h}(\vartheta_{n,m}^{az}-\tilde{\vartheta}_l^{az}) \end{aligned} \tag{55}$$

where $J_{s,nm}^{h/v}$ and $J_{e,nm}^{h/v}$ are start and end column/row indexes of Rx antennas, respectively, which describe the VR of MPCs on the Rx array. Derivations of (54) and (55) are omitted due to the space limitation.

B. ULAs at Both Ends

When uniform linear arrays (ULAs) are employed at the Tx and Rx, by setting $P_v = Q_v = 1$, the beam domain channel elements associated with the jth AoD and the lth AoA are given as

$$\begin{aligned} &h_{B,j,l}^{\mathrm{WV}}(t,f) \\ &\quad= \frac{1}{\sqrt{PQ}} \sum_{n\in\mathcal{B}_{\mathrm{WV}}} \sum_{m=1}^{M_n} \beta_{n,m}\cdot e^{j[2\pi(\nu_{n,m}t - f\tau_{n,m})+\Phi_{n,m}]} \\ &\qquad\times f_{1,P}(\theta_{n,m}^{az}-\tilde{\theta}_j^{az})\cdot f_{1,Q}(\vartheta_{n,m}^{az}-\tilde{\vartheta}_l^{az}) \end{aligned} \tag{56}$$

$$\begin{aligned} &h_{B,j,l}^{\mathrm{PV}}(t,f) \\ &\quad= \frac{1}{\sqrt{PQ}} \sum_{n\in\mathcal{B}_{\mathrm{PV}}} \sum_{m=1}^{M_n} \beta_{n,m}\cdot e^{j[2\pi(\nu_{n,m}t - f\tau_{n,m})+\Phi_{n,m}]} \\ &\qquad\times f_{I_{s,nm},I_{e,nm}}(\theta_{n,m}^{az}-\tilde{\theta}_j^{az}) f_{J_{s,nm},J_{e,nm}}(\vartheta_{n,m}^{az}-\tilde{\vartheta}_l^{az}). \end{aligned} \tag{57}$$

The above result reveals that the linear array only has angular resolution in one dimension. However, the planar array can resolve waves in two dimensions. Note that the (sub)superscripts "h" are omitted for simplicity.

V. Results and Analysis

In this section, results of the proposed BDCM are presented. The impacts of array non-stationarity on beam domain channel characteristics are investigated by comparing the statistics and capacities of the proposed BDCM with those of traditional BDCM (by imposing $\eta = 0$), GBSM, and measurement results. Unless otherwise specified, the following parameters are chosen in simulations: $f_c = 11$ GHz, $N_f = 51$, $W = 160$ MHz, $P_{\mathrm{out}} = 0.1$, $\rho = 10$ dB, $\alpha = \pi/6$, and $v = 5$ m/s. The parameters of MPCs such as powers, delays, and angles are generated according to 3GPP TR38.901 in the indoor NLoS scenario [39]. The VR-related parameters are set according to channel measurements: $\lambda_C^h = 0.112$, $\lambda_C^v = 0.127$, $\lambda_M^{h(v)} = 4.07$, and $\eta = 0.45$ [13], [14].

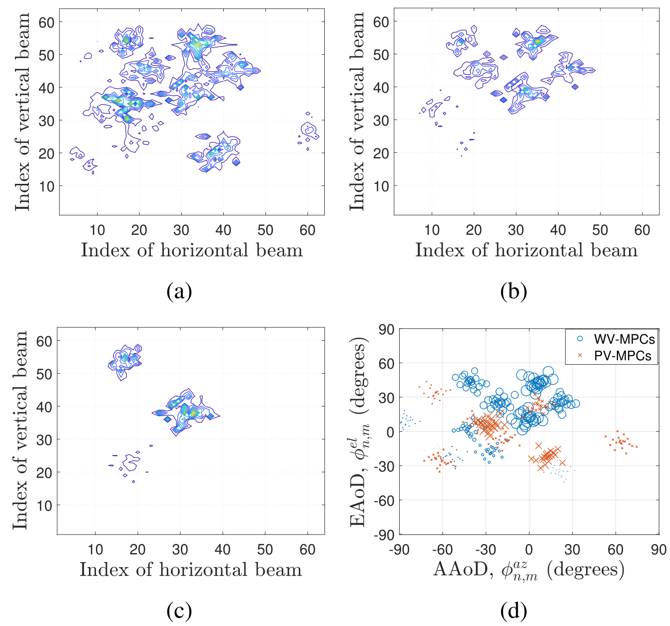

Fig. 4. Contour plots of $|\mathbf{H}_B|$ for (a) traditional BDCM, (b) proposed BDCM for $\eta = 0.45$, and (c) proposed BDCM for $\eta = 0.8$. (d): Angular distribution of MPCs with $\eta = 0.45$.

Figs. 4(a)–(c) show the contour plots of $|\mathbf{H}_B|$ for traditional BDCM and proposed BDCM with different PV-cluster percentages using a 64×64 UPA. The angular distribution of MPCs is shown in Fig. 4(d), where markers "o" and "x" indicate the WV-MPCs and PV-MPCs, respectively. The sizes of marker represent the relative powers of MPCs. Note that the proposed BDCM can be simplified to the traditional BDCM by imposing $\eta = 0$. For purpose of comparison, other model parameters and system configurations are kept the same. In Fig. 4(a), the MPCs for different directions can be well resolved due to the large spatial resolution. Fig. 4(b) is generated considering both WV- and PV-MPCs by setting $\eta = 0.45$, which decreases the spatial resolutions for the directions of PV-MPCs due to the partially visible property. For example, compared to Fig. 4(a), the beams around $(40, 20)$ become indiscernible, which correspond to the PV-cluster centering around $(15^\circ, -20^\circ)$ in Fig. 4(d). Fig. 4(c) is generated by setting $\eta = 0.8$. As η increases, only a small number of beams can be well resolved. The results indicate that the array non-stationarity of massive MIMO channel can increase the beamwidth and decrease the spatial resolution for the directions of PV-MPCs.

Fig. 5(a) shows the power leakage of the proposed BDCM versus VR length of the MPC. Three types of UPA, i.e., 4×32, 4×48, and 4×64, are used for testing. Due to the small number of antennas in elevation, clusters are only evolved in azimuth direction. It is shown that the power leakage reduces as the

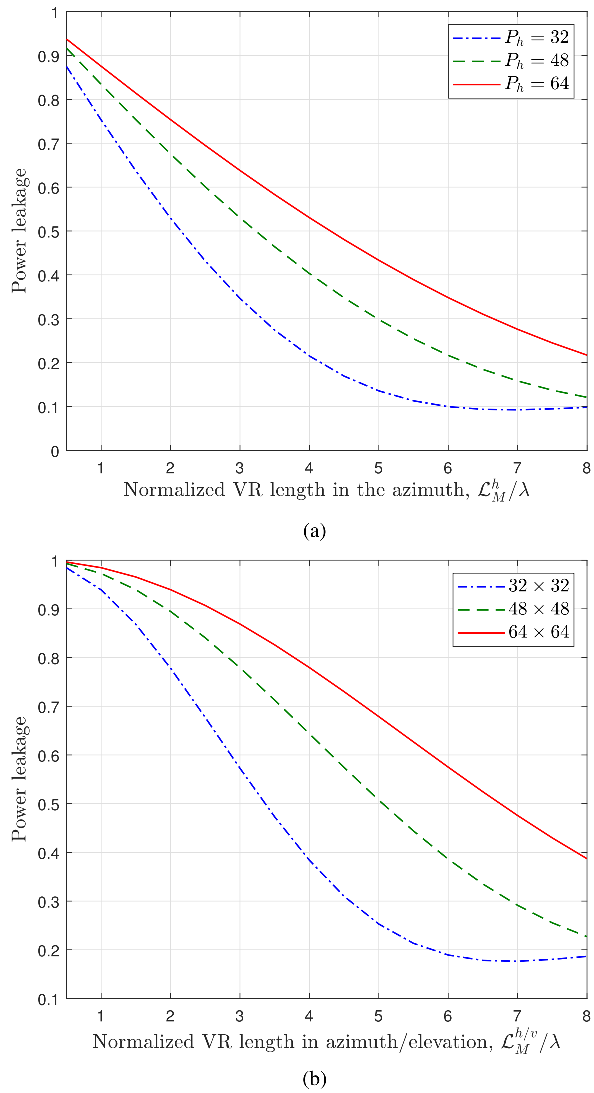

Fig. 5. Power leakage versus VR length when clusters evolved in (a) horizontal and (b) both horizontal and vertical directions ($K_h = K_v = 4$).

VR length increases. For example, in the 4×32 case, 53% of the power is leaked when the VR length is 2λ. The power leakage reduces to 10% when the VR length is 6λ, i.e., about one third of the array length. Besides, with a given VR length, the power leakage is worse for a larger array. Furthermore, the power leakage becomes more severe when cluster evolutions occur in both azimuth and elevation directions. As is shown in Fig. 5(b), where 32×32, 48×48, and 64×64 UPAs are used in the simulations. A VR with 2λ in azimuth and elevation on the 32×32 UPA can lead to nearly 80% power leakage. For the 48×48 UPA, the power leakage further increases to 90%. Note that in traditional BDCMs, all the clusters are considered as WV-clusters that have VRs covering the entire array. This makes the traditional BDCMs underestimate power leakage of the massive MIMO beam domain channel and may lead to inaccurate results in system evaluation.

Fig. 6 shows the comparison of proposed BDCM, traditional BDCM, proposed GBSM, and traditional GBSM in terms of spatial, temporal, and frequency CFs using a 4×64 UPA. The spatial CFs shown in Fig. 6(a) reveal that when

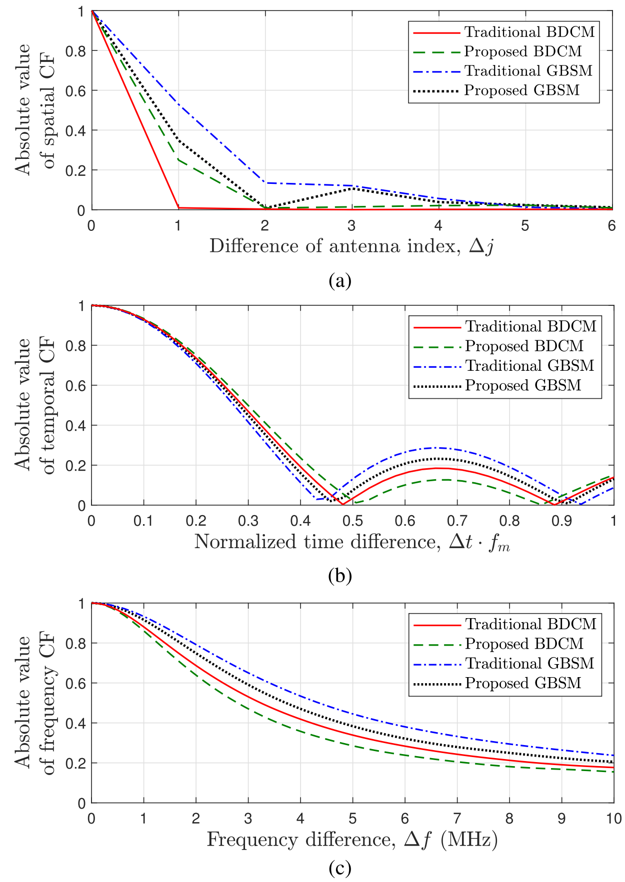

Fig. 6. Comparison of proposed BDCM, traditional BDCM, proposed GBSM, and traditional GBSM in terms of (a) spatial CF, (b) temporal CF, and (c) frequency CF.

array non-stationarity is neglected, the beam domain channel elements are approximately uncorrelated, which is consistent with the analysis in (47). For the proposed BDCM, the spatial correlation increases due to the wide beamwidths stemming from PV-MPCs. For the GBSM, array non-stationarity is shown to have an opposite effect. The reason is that a visible MPC may become invisible over the distance $\Delta j \cdot d_h$, which in turn decreases spatial correlation of the GBSM. Figs. 6(b) and (c) show the temporal and frequency CFs, respectively. For the BDCM and GBSM, the impacts of array non-stationarity stem from different reasons. In the BDCM, the array non-stationarity increases the beamwidths for the PV-MPC directions, making the power of those MPCs diffuses to adjacent beams. In the GBSM, a larger η implies a smaller number of MPCs between Tx and Rx antennas, which in turn influences the temporal and frequency CFs.

Fig. 7(a) shows the azimuth beam spread of the proposed BDCM, azimuth angular spread of the proposed GBSM, and measurement result in [14]. The measurement was conducted at 11 GHz in a theater scenario using a 256-element virtual UPA with two array configurations, i.e., 64×4 and 4×64. Model parameters μ_{lgASD}, σ_{lgASD}, and c_{ASD} are optimized by fitting the angular spread to measurement data, where μ_{lgASD} and σ_{lgASD} are mean and standard deviation of the AAoD spread lognormal distribution in the cluster level, c_{ASD} is AAoD spread within a cluster [39]. For the BDCM with

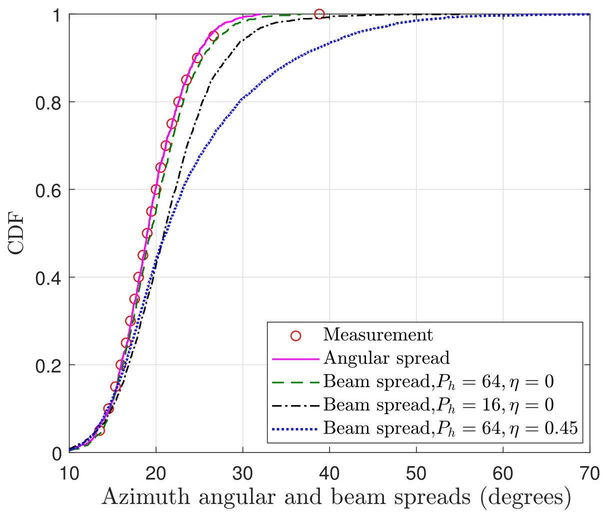

(a)

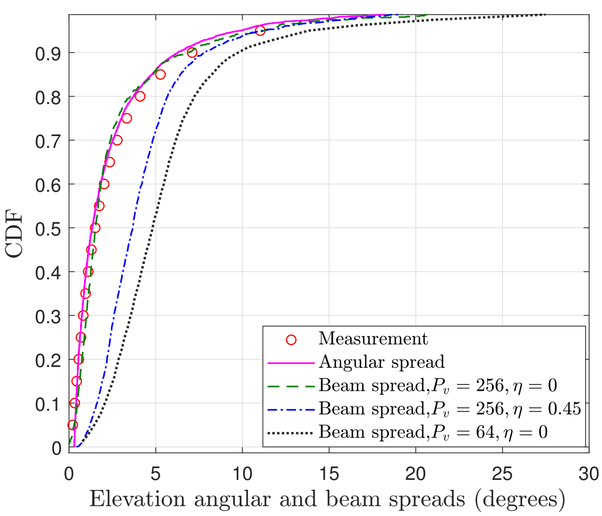

(b)

Fig. 7. Comparison of beam spread, angular spread, and measurement result [14] in (a) azimuth and (b) elevation ($\mu_{\text{lgASD}} = 1.296°$, $\sigma_{\text{lgASD}} = 0.067°$, $c_{\text{ASD}} = 5°$, $\mu_{\text{lgESD}} = 0.086°$, $\sigma_{\text{lgESD}} = 0.528°$, $c_{\text{ESD}} = 0.3°$).

$P_h = 16$ and $\eta = 0$, the beam spread is found to be larger than the angular spread and measurement result. This is caused by the finite spatial resolution of the array, leading to the power of the MPC diffuses to several beams. As the number of antennas increases, i.e, $P_h = 64$, the power leakage is approximatively eliminated. This results in a good fit among the beam spread, angular spread, and the measurement result, showing the correctness and practicability of the proposed model. For $\eta = 0.45$, the beam spread is shown to be significantly larger than aforementioned results due to the severe power leakage.

The elevation beam spread, elevation angular spread, and measurement result are illustrated in Fig. 7(b). Compared with azimuth cases in Fig. 7(a), there is a large discrepancy between the angular spread and beam spread for $P_v = 64$, $\eta = 0$. The underlying reason is that the elevation angular spread is smaller than azimuth angular spread. In other words, the MPCs are more concentrated in elevation than in azimuth. The MPC discrimination relies on a larger dimension of array, i.e., a higher spatial resolution in elevation. Again, the consistency among measurement result, angular spread, and beam spread ($P_v = 256$, $\eta = 0$) can be observed, indicating the correctness and practicability of the proposed model. Similar to the azimuth beam spread, the elevation beam spread increases when the array non-stationarity is taken into consideration. Results suggest that traditional BDCMs neglecting array non-stationary may underestimate the power dispersion of the channel in the beam domain.

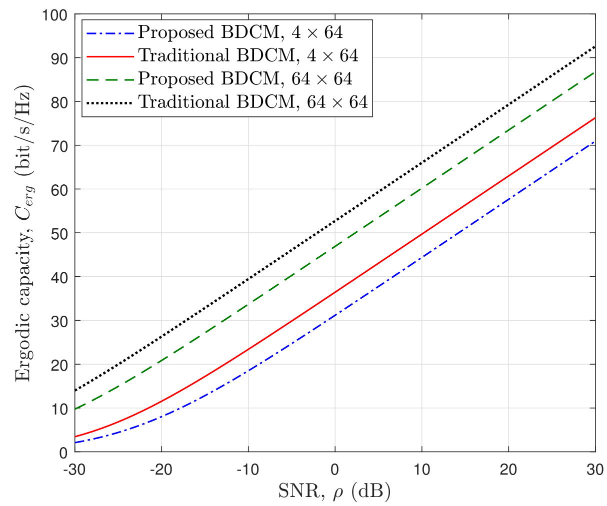

Fig. 8. Ergodic capacities of the proposed and traditional BDCMs with different UPAs.

Fig. 8 shows the comparison of ergodic capacities of the proposed BDCM and traditional BDCM. The UT is equipped with a 1×4 ULA and two types of UPA, i.e., 4×64 and 64×64, are deployed on the BS, accounting for the scenarios where cluster evolution occurs in horizontal and both horizontal and vertical directions, respectively. The ergodic capacities are obtained by averaging 1000 channel realizations and each realization is normalized and fulfills $\sum_{n,m=1}^{N,M_n} \beta_{n,m}^2 = PQ$. We find that for both types of UPA, the capacities of the proposed BDCM are lower than those of the traditional BDCM. The underlying reason is that in traditional BDCM, each cluster can be observed by the whole array, which results in a lower correlation of beam domain channel elements. The result indicates that the traditional BDCMs neglecting array non-stationarity may overestimate the capacity of the beam domain channel.

Fig. 9 illustrates the impact of PV-cluster percentage and VR length on ergodic capacity of the BDCM using a 4×64 UPA. The sizes of VR length are determined by setting $\lambda_C^h = 0.112$ and $\lambda_C^h = 0.037$. The former are obtained from an indoor massive MIMO channel measurement [13] and the latter is set as one-third of the former, making the average value of VR lengths three times longer than the former one. In each case, the model is evaluated using three PV-cluster percentages, i.e., $\eta = 0.45$, $\eta = 0.8$, and $\eta = 1$. Results show that a lower PV-cluster percentage leads to a larger channel capacity. For a given PV-cluster percentage, a small value of λ_C^h implies larger VRs, which further improve the channel capacity.

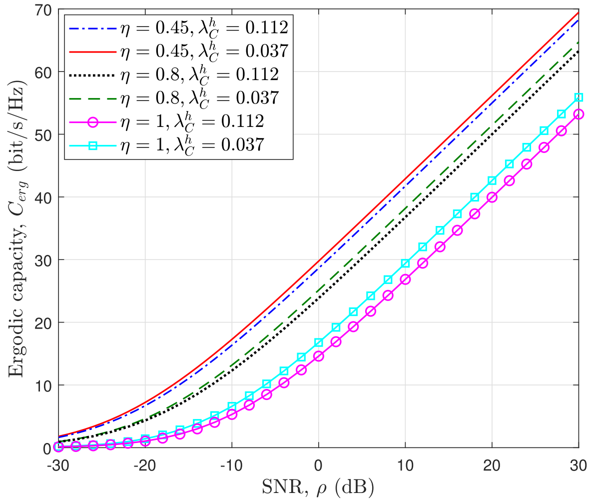

Fig. 9. Ergodic capacity with different VR lengths and PV-cluster percentages.

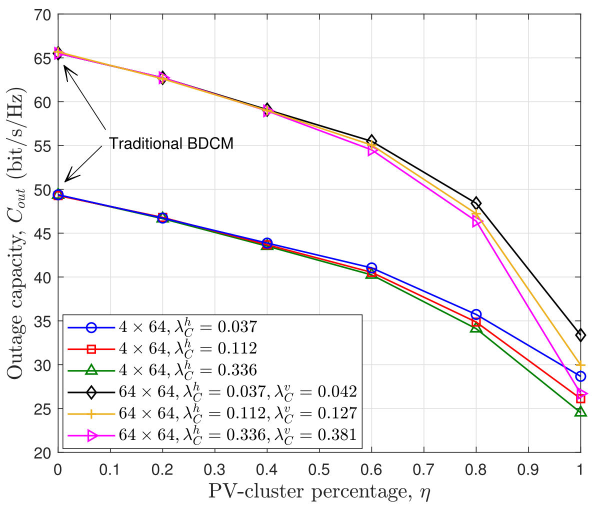

Fig. 10. Outage capacity as a function of the PV-cluster percentage with different VR lengths.

Fig. 10 shows the 0.1 outage capacity as a function of η. We observe that the capacities decrease rapidly for large values of η. For example, in 4×64, $\lambda_C^h = 0.112$ case, increasing η from 0 to 0.6 decreases the capacity from 49.38 to 40.53 bit/s/Hz. However, increasing η from 0.6 to 1 decreases the capacity from 40.53 to 26.12 bit/s/Hz. Besides, for large values of η, the capacities decrease more rapidly for 64×64 UPA than the capacities for 4×64 UPA. The reason is that for 64×64 UPA, cluster evolution occurs both horizontally and vertically. The results shown in this figure differ from those of traditional BDCM in which η is fixed at zero. Furthermore, it is observed that a small value of $\lambda_C^{h(v)}$ leads to a larger capacity when $\eta > 0.6$. However, $\lambda_C^{h(v)}$ has a negligible effect on the capacity when η is relatively small. This suggests that in massive MIMO beam domain systems, the impacts of VR length on system performance cannot be omitted, especially for the scenarios where the array non-stationarity is significant.

VI. Conclusion

This paper has proposed a novel BDCM which has the ability to represent the effects of array non-stationarity of massive MIMO channels. This is achieved by introducing the spatially consistent VRs over the large UPA at the level of MPCs. Statistics including channel power, power leakage, and STF-CF have been obtained. Besides, a novel statistic called beam spread has been proposed to describe the power dispersion of the channel in the beam domain. The correctness and practicability of the proposed BDCM have been validated by comparing it with the corresponding GBSM and measurement results. We have found that the partially visible property of MPCs increases the corresponding beamwidth, which makes the beamwidths and spatial resolutions of the BDCM for different directions not equal. Results have suggested that the traditional BDCMs neglecting the array non-stationarity of massive MIMO channels can underestimate the power leakage and the correlation between channel elements, and overestimate the beam domain channel capacity. Note that the proposed model neglects the variations of amplitudes and angles of MPCs over the array. This simplifies the model and helps in analyzing the impacts of array non-stationarity on beam domain channel behavior. The BDCM incorporating the effects of scatterer visibility and variations of MPC parameters over the array could be a topic for our future research.

Appendix

A. Derivations of (31) *and* (32)

Substituting (19) into (25) and using the equality $(\mathbf{A}\otimes\mathbf{B})(\mathbf{C}\otimes\mathbf{D}) = (\mathbf{AC})\otimes(\mathbf{BD})$, $\mathbf{H}_B^{\mathrm{WV}}(t,f)$ are derived as

$$\mathbf{H}_B^{\mathrm{WV}}(t,f) = \sum_{n\in\mathcal{B}_{\mathrm{WV}}}\sum_{m=1}^{M_n}\beta_{n,m}e^{j[2\pi(\nu_{n,m}t-f\tau_{n,m})+\Phi_{n,m}]} \times[\mathbf{b}^{\mathrm{T}}(\theta_{n,m}^{el})\tilde{\mathbf{U}}_{el}^{*}]\otimes[\mathbf{a}^{\mathrm{T}}(\theta_{n,m}^{az})\tilde{\mathbf{U}}_{az}^{*}]. \quad (58)$$

The element in $\mathbf{H}_B^{\mathrm{WV}}(t,f)$ corresponding to the jth AAoD and the ith EAoD is calculated as

$$\begin{aligned} h_{B,ij}^{\mathrm{WV}}(t,f) &= \sum_{n\in\mathcal{B}_{\mathrm{WV}}}\sum_{m=1}^{M_n}\beta_{n,m}e^{j[2\pi(\nu_{n,m}t-f\tau_{n,m})+\Phi_{n,m}]} \\ &\quad\times\left(\mathbf{b}^{\mathrm{T}}(\theta_{n,m}^{el})[\tilde{\mathbf{U}}_{el}^{*}]_{:,i}\right)\left(\mathbf{a}^{\mathrm{T}}(\theta_{n,m}^{az})[\tilde{\mathbf{U}}_{az}^{*}]_{:,j}\right) \\ &= \sum_{n\in\mathcal{B}_{\mathrm{WV}}}\sum_{m=1}^{M_n}\beta_{n,m}e^{j[2\pi(\nu_{n,m}t-f\tau_{n,m})+\Phi_{n,m}]} \\ &\quad\times\frac{1}{\sqrt{P_v}}\sum_{a=0}^{P_v-1}e^{j2\pi a(\theta_{n,m}^{el}-\tilde{\theta}_i)} \\ &\quad\times\frac{1}{\sqrt{P_h}}\sum_{b=0}^{P_h-1}e^{j2\pi b(\theta_{n,m}^{az}-\tilde{\theta}_j)} \\ &= \frac{1}{\sqrt{P}}\sum_{n\in\mathcal{B}_{\mathrm{WV}}}\sum_{m=1}^{M_n}\beta_{n,m}e^{j[2\pi(\nu_{n,m}t-f\tau_{n,m})+\Phi_{n,m}]} \\ &\quad\times f_{1,P_v}(\theta_{n,m}^{el}-\tilde{\theta}_i^{el})\cdot f_{1,P_h}(\theta_{n,m}^{az}-\tilde{\theta}_j^{az}). \quad (59)\end{aligned}$$

Similarly, by substituting (20) into (25), the element of $\mathbf{H}_B^{\mathrm{PV}}(t,f)$ corresponding to the jth AAoD and the ith EAoD

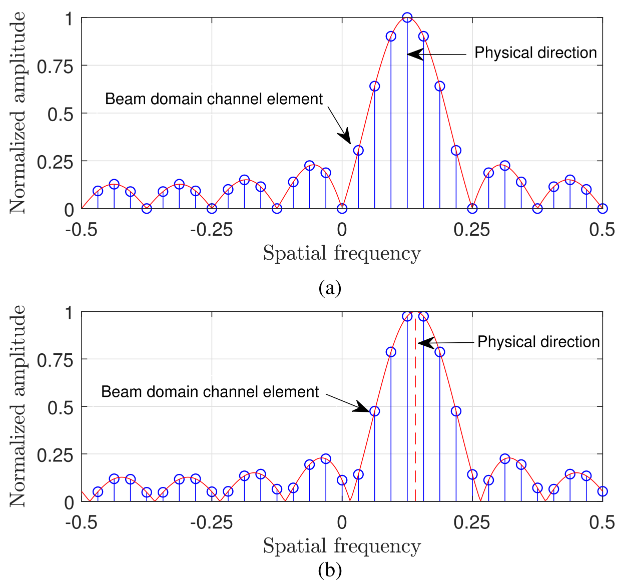

Fig. 11. Illustrations of the power leakage in two special cases, (a) Case I: the physical direction of the PV-MPC is perfectly sampled; (b) Case II: the sample points are uniformly distributed around the physical direction.

is derived as

$$\begin{aligned} h_{B,ij}^{\mathrm{PV}}(t,f) &= \sum_{n\in\mathcal{B}_{\mathrm{PV}}}\sum_{m=1}^{M_n}\beta_{n,m}e^{j[2\pi(\nu_{n,m}t-f\tau_{n,m})+\Phi_L]} \\ &\quad\times\left(\hat{\mathbf{b}}(\theta_{n,m}^{el})^{\mathrm{T}}[\tilde{\mathbf{U}}_{el}^{*}]_{:,i}\right)\left(\hat{\mathbf{a}}(\theta_{n,m}^{az})^{\mathrm{T}}[\tilde{\mathbf{U}}_{az}^{*}]_{:,j}\right) \\ &= \sum_{n\in\mathcal{B}_{\mathrm{PV}}}\sum_{m=1}^{M_n}\beta_{n,m}e^{j[2\pi(\nu_{n,m}t-f\tau_{n,m})+\Phi_{n,m}]} \\ &\quad\times\frac{1}{\sqrt{P_v}}\sum_{a=I_{s,nm}^{v}-1}^{I_{e,nm}^{v}-1}e^{j2\pi a(\theta_{n,m}^{el}-\tilde{\theta}_i)} \\ &\quad\times\frac{1}{\sqrt{P_h}}\sum_{b=I_{s,nm}^{h}-1}^{I_{e,nm}^{h}-1}e^{j2\pi b(\theta_{n,m}^{az}-\tilde{\theta}_j)}=\frac{1}{\sqrt{P}}\sum_{n\in\mathcal{B}_{\mathrm{PV}}} \\ &\quad\sum_{m=1}^{M_n}\beta_{n,m}e^{j[2\pi(\nu_{n,m}t-f\tau_{n,m})+\Phi_{n,m}]}f_{I_{s,nm}^{v},I_{e,nm}^{v}} \\ &\quad\times(\theta_{n,m}^{el}-\tilde{\theta}_i^{el})f_{I_{s,nm}^{h},I_{e,nm}^{h}}(\theta_{n,m}^{az}-\tilde{\theta}_j^{az}). \end{aligned} \tag{60}$$

B. Derivation of (40)

We start with the simple $1\times P_h$ ULA case. As is shown in Fig. 11, the normalized amplitudes of channel elements in $\mathbf{H}_B$ distribute over a 32-element ULA, where the VR of the MPC covers 8 consecutive antennas. The power leakage can be measured by considering two cases, i.e., Case I: the physical direction of the MPC is perfectly sampled, which is shown in Fig. 11(a), and Case II: the sample points are uniformly distributed on the two sides of the physical direction, which is shown in Fig. 11(b). It can be observed that the power leakages are inevitable in both cases due to the partial visibility of MPC and are asymptotically equal as the number of antenna elements tends to infinity. For instance, the power leakage for Case II is calculated as

$$\Gamma = 1-\frac{\sum_{j\in\mathcal{U}(\theta_0^{az},K_h)}\left|h_{B,j}^{\mathrm{PV}}\right|^2}{\sum_{j=1}^{P_h}\left|h_{B,j}^{\mathrm{PV}}\right|^2} \tag{61}$$

where

$$\begin{aligned} &\mathcal{U}(\theta_0,K_h)= \\ &\left\{j:\left(\theta_0-\frac{K_h}{2P_h}\right)\bmod 1\leqslant\tilde{\theta}_j<\left(\theta_0+\frac{K_h}{2P_h}\right)\bmod 1\right\}. \end{aligned} \tag{62}$$

Note that the spatial frequencies are equally spaced at $1/P_h$. By substituting (32) into (61) and imposing $I_s^v=I_e^v=1$, the power leakage is obtained as

$$\begin{aligned} \Gamma &= 1-\frac{\sum_{j=0}^{K_h/2-1}D_{I_e-I_s+1}^2\left(\frac{2j+1}{2P_h}\right)}{\sum_{j=0}^{P_h/2-1}D_{I_e-I_s+1}^2\left(\frac{2j+1}{2P_h}\right)} \\ &= 1-\frac{2\sum_{j=0}^{K_h/2-1}D_{I_e-I_s+1}^2\left(\frac{2j+1}{2P_h}\right)}{(I_e-I_s+1)P_h}. \end{aligned} \tag{63}$$

The right side of the second equal sign is derived based on the Parseval's theorem. The power leakage for the UPA case in (40) can be obtained by substituting (32) into (39) and following a similar procedure.

REFERENCES

[1] X. You *et al.*, "Towards 6G wireless communication networks: Vision, enabling technologies, and new paradigm shifts," *Sci. China Inf. Sci.*, vol. 64, no. 1, pp. 110301–110374, Jan. 2021.
[2] J. Wang, C.-X. Wang, J. Huang, H. Wang, and X. Gao, "A general 3D space-time-frequency non-stationary THz channel model for 6G ultra-massive MIMO wireless communication systems," *IEEE J. Sel. Areas Commun.*, vol. 39, no. 6, pp. 1576–1589, Jun. 2021.
[3] L. You, J. Wang, W. Wang, and X. Gao, "Secure multicast transmission for massive MIMO with statistical channel state information," *IEEE Signal Process. Lett.*, vol. 26, no. 6, pp. 803–807, Jun. 2019.
[4] C.-X. Wang, Z. Lv, X. Q. Gao, X. You, Y. Hao, and H. Haas, "Pervasive wireless channel modeling theory and applications to 6G GBSMs for all frequency bands and all scenarios," *IEEE Trans. Veh. Technol.*, early access, Jun. 2, 2022, doi: 10.1109/TVT.2022.3179695.
[5] C. Sun, X. Q. Gao, S. Jin, M. Matthaiou, Z. Ding, and C. Xiao, "Beam division multiple access transmission for massive MIMO communications," *IEEE Trans. Commun.*, vol. 63, no. 6, pp. 2170–2184, Jun. 2015.
[6] L. You, X. Gao, G. Y. Li, X.-G. Xia, and N. Ma, "BDMA for millimeter-wave/terahertz massive MIMO transmission with per-beam synchronization," *IEEE J. Sel. Areas Commun.*, vol. 35, no. 7, pp. 1550–1563, Jul. 2017.
[7] C. Huang *et al.*, "Holographic MIMO surfaces for 6G wireless networks: Opportunities, challenges, and trends," *IEEE Wireless Commun.*, vol. 27, no. 5, pp. 118–125, Oct. 2020.
[8] J. Huang *et al.*, "Reconfigurable intelligent surfaces: Channel characterization and modeling," *Proc. IEEE*, to be published.
[9] X. Wei, D. Shen, and L. Dai, "Channel estimation for RIS assisted wireless communications—Part I: Fundamentals, solutions, and future opportunities," *IEEE Commun. Lett.*, vol. 25, no. 5, pp. 1398–1402, May 2021.
[10] J. Bian, C.-X. Wang, X. Q. Gao, X. You, and M. Zhang, "A general 3D non-stationary wireless channel model for 5G and beyond," *IEEE Trans. Wireless Commun.*, vol. 20, no. 5, pp. 3211–3224, May 2021.
[11] A. O. Martínez, E. D. Carvalho, and J. Ø. Nielsen, "Towards very large aperture massive MIMO: A measurement based study," in *Proc. IEEE GC Wkshps*, Austin, TX, USA, Dec. 2014, pp. 281–286.
[12] Q. Wang *et al.*, "Spatial variation analysis for measured indoor massive MIMO channels," *IEEE Access*, vol. 5, pp. 20828–20840, 2017.
[13] J. Li *et al.*, "On 3D cluster-based channel modeling for large-scale array communications," *IEEE Trans. Wireless Commun.*, vol. 18, no. 10, pp. 4902–4914, Oct. 2019.

[14] J. Li, B. Ai, R. He, M. Yang, Z. Zhong, and Y. Hao, "A cluster-based channel model for massive MIMO communications in indoor hotspot scenarios," *IEEE Trans. Wireless Commun.*, vol. 18, no. 8, pp. 3856–3870, Aug. 2019.

[15] J. Bian, C.-X. Wang, Y. Liu, J. Tian, J. Qiao, and X. Zheng, "3D non-stationary wideband UAV-to-ground MIMO channel models based on aeronautic random mobility model," *IEEE Trans. Veh. Technol.*, vol. 70, no. 11, pp. 11154–11168, Nov. 2021.

[16] X. Zhu, C.-X. Wang, J. Huang, M. Chen, and H. Haas, "A novel 3D non-stationary channel model for 6G indoor visible light communication systems," *IEEE Trans. Wireless Commun.*, early access, Apr. 20, 2022, doi: 10.1109/TWC.2022.3165569.

[17] Y. He *et al.*, "A novel 3D non-stationary maritime wireless channel model," *IEEE Trans. Commun.*, vol. 70, no. 3, pp. 2102–2116, Mar. 2022.

[18] Y. Liu, C.-X. Wang, H. Chang, Y. He, and J. Bian, "A novel non-stationary 6G UAV channel model for maritime communications," *IEEE J. Sel. Areas Commun.*, vol. 39, no. 10, pp. 2992–3005, Oct. 2021.

[19] C. F. Lopez and C.-X. Wang, "Novel 3-D non-stationary wideband models for massive MIMO channels," *IEEE Trans. Wireless Commun.*, vol. 17, no. 5, pp. 2893–2905, May 2018.

[20] S. Wu, C.-X. Wang, E.-H. M. Aggoune, M. M. Alwakeel, and X. You, "A general 3-D non-stationary 5G wireless channel model," *IEEE Trans. Commun.*, vol. 66, no. 7, pp. 3065–3078, Jul. 2018.

[21] X. Li, S. Zhou, E. Björnson, and J. Wang, "Capacity analysis for spatially non-wide sense stationary uplink massive MIMO systems," *IEEE Trans. Wireless Commun.*, vol. 14, no. 12, pp. 7044–7056, Dec. 2015.

[22] C. F. Lopez, C.-X. Wang, and Y. Zheng, "A 3D non-stationary wideband massive MIMO channel model based on ray-level evolution," *IEEE Trans. Commun.*, vol. 70, no. 1, pp. 621–634, Jan. 2022.

[23] G. N. Kamga, M. Xia, and S. Aïssa, "Spectral-efficiency analysis of regular- and large-scale (massive) MIMO with a comprehensive channel model," *IEEE Trans. Veh. Technol.*, vol. 66, no. 6, pp. 4984–4996, Jun. 2017.

[24] K. Dovelos, M. Matthaiou, H. Q. Ngo, and B. Bellalta, "Massive MIMO with multi-antenna users under jointly correlated Ricean fading," in *Proc. IEEE ICC*, Dublin, Ireland, Jun. 2020, pp. 1–6.

[25] Z. Shen, K. Xu, and X. Xia, "Beam-domain anti-jamming transmission for downlink massive MIMO systems: A Stackelberg game perspective," *IEEE Trans. Inf. Forensics Security*, vol. 16, pp. 2727–2742, 2021.

[26] X. Gao, L. Dai, S. Zhou, A. M. Sayeed, and L. Hanzo, "Wideband beamspace channel estimation for millimeter-wave MIMO systems relying on lens antenna arrays," *IEEE Trans. Signal Process.*, vol. 67, no. 18, pp. 4809–4824, Sep. 2019.

[27] W. Shen, X. Bu, X. Gao, C. Xing, and L. Hanzo, "Beamspace precoding and beam selection for wideband millimeter-wave MIMO relying on lens antenna arrays," *IEEE Trans. Signal Process.*, vol. 67, no. 24, pp. 6301–6313, Dec. 2019.

[28] X. Gao, L. Dai, Y. Zhang, T. Xie, X. Dai, and Z. Wang, "Fast channel tracking for terahertz beamspace massive MIMO systems," *IEEE Trans. Veh. Technol.*, vol. 66, no. 7, pp. 5689–5696, Jul. 2017.

[29] S. Wu, C. X. Wang, H. Haas, E. H. M. Aggoune, M. M. Alwakeel, and B. Ai, "A non-stationary wideband channel model for massive MIMO communication systems," *IEEE Trans. Wireless Commun.*, vol. 14, no. 3, pp. 1434–1446, Mar. 2015.

[30] H. Chang *et al.*, "A novel nonstationary 6G UAV-to-ground wireless channel model with 3-D arbitrary trajectory changes," *IEEE Int. Things J.*, vol. 8, no. 12, pp. 9865–9877, Jun. 2021.

[31] J. Huang, C.-X. Wang, R. Feng, J. Sun, W. Zhang, and Y. Yang, "Multi-frequency mmWave massive MIMO channel measurements and characterization for 5G wireless communication systems," *IEEE J. Sel. Areas Commun.*, vol. 35, no. 7, pp. 1591–1605, Jul. 2017.

[32] J. Brady, N. Behdad, and A. M. Sayeed, "Beamspace MIMO for millimeter-wave communications: System architecture, modeling, analysis, and measurements," *IEEE Trans. Antennas Propag.*, vol. 61, no. 7, pp. 3814–3827, Jul. 2013.

[33] J. Huang, C.-X. Wang, H. Chang, J. Sun, and X. Q. Gao, "Multi-frequency multi-scenario millimeter wave MIMO channel measurements and modeling for B5G wireless communication systems," *IEEE J. Sel. Areas Commun.*, vol. 38, no. 9, pp. 2010–2025, Sep. 2020.

[34] N. Czink, P. Cera, J. Salo, E. Bonek, J.-P. Nuutinen, and J. Ylitalo, "Improving clustering performance using multipath component distance," *Electron. Lett.*, vol. 42, no. 1, pp. 33–35, Jan. 2006.

[35] P. Kyösti *et al.*, *WINNER II Channel Models*, document IST-4-027756, WINNER II D1.1.2, Version 1.2, Apr. 2008.

[36] T. Xie, L. Dai, D. W. K. Ng, and C.-B. Chae, "On the power leakage problem in millimeter-wave massive MIMO with lens antenna arrays," *IEEE Trans. Signal Process.*, vol. 67, no. 18, pp. 4730–4744, Sep. 2019.

[37] Z. Xia, C. Qi, and T. Zhang, "Model based beamspace channel estimation for millimeter wave massive MIMO system," in *Proc. WCSP*, Hangzhou, China, Oct. 2018, pp. 1–6.

[38] W. Q. Malik, "MIMO capacity convergence in frequency-selective channels," *IEEE Trans. Commun.*, vol. 57, no. 2, pp. 353–356, Feb. 2009.

[39] *Study on Channel Model for Frequencies From 0.5 to 100 GHz*, document TR 38.901, Version 17.0.0, 3GPP, Mar. 2022.

Ji Bian (Member, IEEE) received the B.Sc. degree in electronic information science and technology from Shandong Normal University, Jinan, Chian, in 2010, the M.Sc. degree in signal and information processing from the Nanjing University of Posts and Telecommunications, Nanjing, China, in 2013, and the Ph.D. degree in information and communication engineering from Shandong University, Jinan, in 2019. From 2017 to 2018, he was a Visiting Scholar with the School of Engineering and Physical Sciences, Heriot-Watt University, Edinburgh, U.K. He is currently a Lecturer with the School of Information Science and Engineering, Shandong Normal University. His research interests include 6G channel modeling and wireless big data.

Cheng-Xiang Wang (Fellow, IEEE) received the B.Sc. and M.Eng. degrees in communication and information systems from Shandong University, Jinan, China, in 1997 and 2000, respectively, and the Ph.D. degree in wireless communications from Aalborg University, Aalborg, Denmark, in 2004.

He was a Research Assistant with the Hamburg University of Technology, Hamburg, Germany, from 2000 to 2001; a Visiting Researcher with Siemens AG Mobile Phones, Munich, Germany, in 2004; and a Research Fellow with the University of Agder, Grimstad, Norway, from 2001 to 2005. He has been with Heriot-Watt University, Edinburgh, U.K., since 2005, where he was promoted to a Professor in 2011. In 2018, he joined Southeast University, Nanjing, China, as a Professor. He is also a part-time Professor with Purple Mountain Laboratories, Nanjing. He has authored four books, three book chapters, and more than 480 papers in refereed journals and conference proceedings, including 26 highly cited papers. He has also delivered 24 invited keynote speeches/talks and 14 tutorials in international conferences. His current research interests include wireless channel measurements and modeling, 6G wireless communication networks, and electromagnetic information theory.

Prof. Wang is a member of the Academia Europaea (The Academy of Europe); a member of the European Academy of Sciences and Arts (EASA); a fellow of the Royal Society of Edinburgh (FRSE), IET, and China Institute of Communications (CIC). He is a Highly-Cited Researcher recognized by Clarivate Analytics from 2017 to 2020 and one of the most cited Chinese Researchers recognized by Elsevier in 2021. He received 15 Best Paper Awards from IEEE GLOBECOM 2010, IEEE ICCT 2011, ITST 2012, IEEE VTC 2013Spring, IWCMC 2015, IWCMC 2016, IEEE/CIC ICCC 2016, WPMC 2016, WOCC 2019, IWCMC 2020, WCSP 2020, CSPS2021, WCSP 2021, and IEEE/CIC ICCC 2022. He has served as a TPC member, a TPC chair, and a general chair for more than 80 international conferences. He is currently an Executive Editorial Committee Member of the IEEE TRANSACTIONS ON WIRELESS COMMUNICATIONS. He has served as an Editor for over ten international journals, including the IEEE TRANSACTIONS ON WIRELESS COMMUNICATIONS from 2007 to 2009, the IEEE TRANSACTIONS ON VEHICULAR TECHNOLOGY from 2011 to 2017, and the IEEE TRANSACTIONS ON COMMUNICATIONS from 2015 to 2017. He was the Guest Editor of the IEEE JOURNAL ON SELECTED AREAS IN COMMUNICATIONS, Special Issue on Vehicular Communications and Networks (a Lead Guest Editor), Special Issue on Spectrum and Energy Efficient Design of Wireless Communication Networks, and Special Issue on Airborne Communication Networks. He was also a Guest Editor for the IEEE TRANSACTIONS ON BIG DATA, Special Issue on Wireless Big Data, and the IEEE TRANSACTIONS ON COGNITIVE COMMUNICATIONS AND NETWORKING, Special Issue on Intelligent Resource Management for 5G and Beyond. He is the IEEE Communications Society Distinguished Lecturer in 2019 and 2020.

Rui Feng (Member, IEEE) received the B.Sc. degree in communication engineering and the M.Eng. degree in signal and information processing from Yantai University, China, in 2011 and 2014, respectively, and the Ph.D. degree in communication and information system from Shandong University, China, in 2018. From July 2018 to September 2020, she was a Lecture at Ludong University, China. She is currently a Post-Doctoral Research Associate at Purple Mountain Laboratories and Southeast University, China. Her research interests include ultra-massive MIMO channel modeling theory and beam domain channel modeling.

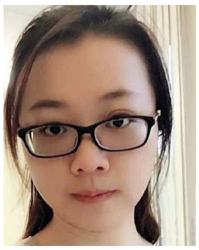

Yu Liu (Member, IEEE) received the Ph.D. degree in communication and information systems from Shandong University, Jinan, China, in 2017. From 2015 to 2017, she was a Visiting Scholar with the School of Engineering and Physical Sciences, Heriot-Watt University, Edinburgh, U.K. From 2017 to 2019, she was a Post-Doctoral Research Associate with the School of Information Science and Engineering, Shandong University. Since 2019, she has been an Associate Professor with the School of Microelectronics, Shandong University. Her main research interests include nonstationary wireless MIMO channel modeling, high speed train wireless propagation characterization and modeling, and channel modeling for special scenarios.

Wenqi Zhou received the B.Sc. degree in electrical engineering and automation from Shandong Construction University, China, in 2001, and the M.Eng. degree in control theory and control engineering from Shandong University, China, in 2006. He is currently pursuing the Ph.D. degree with Southeast University, China.

His research interests include 6G scenario classification and identification and AI-based predictive channel modeling.

Fan Lai (Student Member, IEEE) received the B.E. degree from Dalian Maritime University, Dalian, China, in 2015. He is currently pursuing the Ph.D. degree with the National Mobile Communications Research Laboratory, Southeast University, Nanjing, China. His research interests include massive MIMO channel measurement and modeling and shortwave channel modeling.

Xiqi Gao (Fellow, IEEE) received the Ph.D. degree in electrical engineering from Southeast University, Nanjing, China, in 1997.

He joined the Department of Radio Engineering, Southeast University, in April 1992. Since May 2001, he has been a Professor of information systems and communications. From September 1999 to August 2000, he was a Visiting Scholar at the Massachusetts Institute of Technology, Cambridge, and Boston University, Boston, MA, USA. From August 2007 to July 2008, he visited the Darmstadt University of Technology, Darmstadt, Germany, as a Humboldt scholar. His current research interests include broadband multicarrier communications, massive MIMO wireless communications, satellite communications, optical wireless communications, information theory, and signal processing for wireless communications.

Dr. Gao received the Science and Technology Awards of the State Education Ministry of China in 1998, 2006, and 2009; the National Technological Invention Award of China in 2011; the Science and Technology Award of Jiangsu Province of China in 2014; and the 2011 IEEE Communications Society Stephen O. Rice Prize Paper Award in the field of communications theory. From 2007 to 2012, he served as an Editor for the IEEE TRANSACTIONS ON WIRELESS COMMUNICATIONS. From 2009 to 2013, he served as an Associate Editor for the IEEE TRANSACTIONS ON SIGNAL PROCESSING. From 2015 to 2017, he served as an Editor for the IEEE TRANSACTIONS ON COMMUNICATIONS.